



Aus dem
Leibniz-Institut für Neurobiologie, Magdeburg

Mutations in *NPTN* could hinder neurodevelopment by impairing the regulation of plasma membrane Ca^{2+} -ATPase (PMCA) levels and Ca^{2+} transients in brain neurons

D i s s e r t a t i o n

zur Erlangung des Doktorgrades

Dr. med.

(doctor medicinae)

an der Medizinischen Fakultät
der Otto-von-Guericke-Universität Magdeburg

vorgelegt von Yi Liang

aus Shanxi, China

Magdeburg 2024

“Per aspera ad astra”

穿越逆境，抵达繁星

Documentation

Bibliographic description

Yi Liang: Mutations in *NPTN* could hinder neurodevelopment by impairing the regulation of plasma membrane Ca^{2+} -ATPase (PMCA) levels and Ca^{2+} transients in brain neurons.

-2024., 70 pages, 21 figures, 11 tables

Department

Medical faculty, OVGU, Magdeburg

Leibniz Institute for Neurobiology (LIN) Magdeburg

Abstract

In recent years, the genetic factors of neurodevelopmental disorders (NDDs) are being explored. Recently, mutations in the Neuroplastin gene (*Nptn*, *NPTN*) have been discovered in mice with hearing deficits and in human patients suffering from NDDs. Neuroplastin (Np), is a member of the immunoglobulin superfamily, and its expression is necessary to maintain the expression levels of the calcium pump plasma membrane Ca^{2+} -ATPase (PMCA) and its proper trafficking. This is intimately related to the regulation of intracellular Ca^{2+} homeostasis. So far, no studies have explored the molecular pathogenesis of NDDs caused by *NPTN* gene mutations. In this work, by generating expression constructs, transfecting HEK293T cells and primary hippocampal neurons, employing *in vitro* calcium imaging techniques, and creating mutant *Drosophila melanogaster* lines, the study identified the expression levels of Np and PMCA for each variant, as well as the dynamics of Ca^{2+} extrusion under different conditions (overexpression, low frequency stimulation, high frequency stimulation and Np-siRNA knock down conditions). The results indicated that the missense mutations *pitch* (C315S) and *audio-1* (I122N) in *Nptn*; p.W135R and p.P342L in *NPTN* impaired the structure and function of the Np protein and the PMCA-neuroplastin complex, leading to impaired cellular Ca^{2+} homeostasis. This may be the molecular pathological mechanism causing hearing defects in mice and NDDs in human. This study proposed a molecular mechanism underlying the pathological process of outer hair cell degeneration leading to deafness in *Nptn* mouse mutants and of the NDDs associated *NPTN* human variants. This work deepens our understanding of NDDs and may provide new insights for early detection and further innovative treatments.

Contents

Documentation.....	i
List of Abbreviations.....	1
1. Introduction.....	3
1.1. Neurodevelopmental disorders (NDDs) and related genetic factors.....	3
1.2. Neuroplastin (Np).....	4
1.2.1. Isoforms and structure of Np.....	4
1.2.2. Molecular function of Np and binding partners.....	5
1.3. Plasma membrane Ca ²⁺ ATPases (PMCA).....	7
1.3.1. PMCA and Np.....	7
1.3.2. Np related diseases.....	7
1.3.3. PMCA related diseases.....	8
1.3.4. Np and PMCA function in the hearing system.....	9
1.4. Np's homology in <i>Drosophila</i> -Basigin.....	11
2. Hypothesis and aims of the thesis.....	13
3. Materials and Methods.....	14
3.1. Generation of constructs encoding WT and Mutated Np.....	14
3.1.1. Primer design.....	14
3.1.2. Polymerase Chain Reaction (PCR).....	15
3.1.3. Cold Fusion™-based cloning procedure.....	16
3.1.4. Transformation of bacteria.....	17
3.1.5. Mini preparation and restriction digestion.....	17
3.1.6. Plasmid Midi preparation.....	18
3.2. Human Embryonic Kidney (HEK)293T cell culture.....	18
3.2.1. Transfection of HEK293T cells.....	18
3.2.2. Measurement of protein concentration by Amido Black.....	19
3.3. Western Blot.....	19
3.4. Total RNA isolation and qPCR.....	20
3.5. Culture of hippocampal neurons.....	21
3.6. Transfection of hippocampal neurons.....	21
3.7. Immunocytochemistry in hippocampal neurons.....	21
3.8. Calcium live imaging.....	22
3.9. Generating transgenic flies for expression of hNp55 ^{p.P>L}	23

3.10. Recombination of transgenic lines and Gal4-induced expression.....	23
3.11. Immunohistochemistry in larvae	24
3.12. Confocal microscopy.....	25
3.13. Statistical analysis	25
4. Results.....	26
4.1. Generation of plasmids for the expression of mutated human Np	26
4.2. Reduced expression of mutated human Np and PMCA in HEK293T cells	27
4.3. Altered glycosylation of hNp55/65 ^{audio-1}	30
4.4. Causes of reduced Np expression	31
4.5. Overexpression of mutated Np reduced the expression of hNp and PMCA in neurons and failed to promote endogenous PMCA levels leading to altered basal cytosolic Ca ²⁺ -level restoration in neurons	34
4.6. Np-siRNA knock-down experiments for human variants.....	41
4.7. <i>NPTN</i> p.P>L variant displayed functional deficits in <i>Drosophila</i>	42
5. Discussion	44
5.1. Reduced PMCA and mutant Np protein expression levels are due to accelerated degradation resulting from protein structural changes	44
5.2. The reduction in PMCA expression is caused by the decreased binding capacity of Np and PMCA	46
5.3. <i>NPTN</i> mutations fail to promote endogenous PMCA levels and maintain basal cytosolic Ca ²⁺ restoration in neurons	48
5.4. Expression in <i>Drosophila</i> NMJs model revealed the reduced Np and PMCA in p.P>L mutation under the <i>in vivo</i> system	49
5.5. Potential pathogenesis of mutant Np in auditory deficits and NDDs	50
6. Zusammenfassung	52
7. Bibliography	53
8. Acknowledgements	60
9. Ehrenerklärung	62
10. Curriculum Vitae	64
11. Appendix.....	66

List of Abbreviations

AD	Alzheimer's Disease
AMPA	α -amino-3-hydroxy-5-methyl-4-isoxazolepropionic acid receptor
A β	Amyloid β -peptide
BSA	Bovine serum albumin
Bsg	Basigin
CA	cornu ammonis
CaM	Calmodulin
cDNA	Complementary deoxyribonucleic acid
DG	dentate gyrus
DIV	Day <i>in vitro</i>
DMEM	Dulbecco's Modified Eagle's Medium
DT	Decay Time
E	Embryonic day
E.coli	Escherichia Coli
EDTA	Ethylenediaminetetraacetic acid
ENU	N-ethyl-N-nitrosourea
FGFR	Fibroblast Growth Factor Receptor
GABA _A R	γ -Aminobutyric acid type A receptor
GFP	Green fluorescent protein
HBSS	Hank's Balanced Salt Solution
HEK	Human Embryonic Kidney Cell
HEPES	4-(2-hydroxyethyl)-1-piperazineethanesulfonic acid
HFS	High frequency electrical stimulation
HW	Half width
Ig	Immunoglobulin
IHC	Inner hair cell
LB	Lysogeny broth
LFS	Low frequency electrical stimulation

LTP	Long Term Potentiation
MCT2	Monocarboxylate Transporter 2
NDDs	Neurodevelopmental disorders
NMJ	Neuromuscular junction
Np	Neuroplastin
OC	Corti
OHC	Outer hair cell
P	Postnatal day
p38MAPK	p38 mitogen-activated protein kinases
PA	Peak amplitude
PCR	Polymerase Chain Reaction
PFA	Paraformaldehyde
PMCA	Plasma membrane Ca^{2+} ATPase
ROI	regions of interest
SERCA	Sarco/endoplasmic reticulum Ca^{2+} -ATPase
SGN	Spiral ganglion cells
SNPs	Single nucleotide polymorphisms
SPCA	Secretory pathway Ca^{2+} -ATPase
TM	Transmembrane domain
TRAF	Tumor necrosis factor receptor-associated factor
WT	Wild-type

1. Introduction

1.1. Neurodevelopmental disorders (NDDs) and related genetic factors

NDDs encompass a highly heterogeneous group of diseases characterized by disruptions in the brain's growth and development. These impairments can significantly affect individual's intelligence, language skills, emotional regulation, behavior, self-control, and cognitive abilities, including learning and memory (American Psychiatric Association, 2013). Besides, some neuropsychiatric disorders, such as schizophrenia, bipolar disorder, cerebral palsy and epilepsy were also recently considered to be included (Moreno-De-Luca et al. 2013; Morris-Rosendahl et al. 2020; Reiss 2009).

With the rapid development of molecular biology, genetics and genomics, neuropsychiatric disorders are more frequently categorized based on the underlying molecular biological mechanisms, particularly focusing on the genes and specific genetic variations implicated in their etiology. Several genes and their mutations have been reported to be associated with NDDs. For example, numerous *de novo* mutations have been independently identified associated to autism with genes including *SHANK*, *ARID1B*, *ADNP*, *SYNGAP1* and *CHD8*; associated to schizophrenia with genes including *PTPRG*, *TGM5*, *SLC39A13*, *BTK*, and *CDKN3*, associated to intellectual disability with genes including *GATAD2B* and *SCN2A* (Cardoso et al. 2019).

Interestingly, there are recently a growing number of variant types for the *NPTN* gene listed in databases include missense mutations, synonymous mutations and frameshift mutations (ClinVar, gnomAD). These variants may or may not be necessarily associated with the pathogenicity of *NPTN* which led to NDDs.

It has been reported that *NPTN* is deleted in a chromosomal microdeletion in a patient with autism and patients with developmental delay (15q24 microdeletion syndrome) (Filipek et al. 2003; Klopocki et al. 2008; Sharp et al. 2007). A comprehensive association study conducted with adolescents has suggested that a collective contribution of multiple Single nucleotide polymorphisms (SNPs) within the *NPTN* polymorphism (rs7171755) locus may be significantly associated with the thickness of the left cerebral cortex (Desrivieres et al. 2015). Saito et.al and Smith et al. also found

that *NPTN* may be involved in genetic susceptibility to schizophrenia. (Saito et al. 2007; Smith et al. 2009)

Therefore, further exploration of the molecular mechanisms of pathogenicity in NDDs that may be due to mutations in the *NPTN* gene is highly desirable.

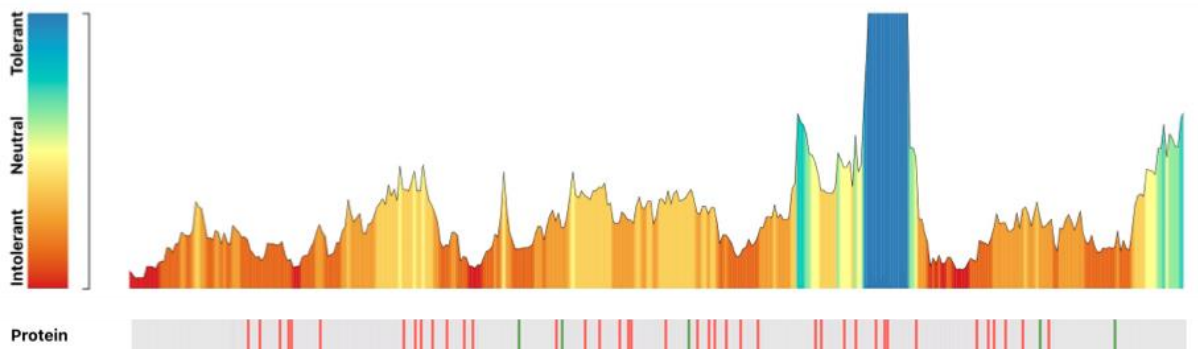


Figure 1: Overview of the variant susceptibility landscape for *NPTN* along with the distribution of variants observed in individuals

Utilizing the MetaDome web server, it has been determined that all amino acid residues affected by missense variants show intolerance to functional genetic alterations (source: MetaDome, <https://stuart.radboudumc.nl/metadome/dashboard>). Accompanying the graph is a schematic representation of *NPTN*, emphasizing the truncating variants identified in patients. Notably, the missense variants highlighted in green were discovered in individuals diagnosed with NDDs within the scope of this study.

1.2. Neuroplastin (Np)

1.2.1. Isoforms and structure of Np

The *NPTN* gene encodes two Np isoforms, with apparent molecular masses of 65 and 55 kDa. Np55 contains two Immunoglobulin domains (Ig) and is widely expressed in nearly all the tissues. However, Np65 has the extra N-terminal specific Ig1 and is specifically expressed in neurons of the brain e.g., in cortex, hippocampus, striatum, cerebellum, thalamus, and hypothalamus at high level (Sakaguchi et al. 2016; Langaese et al. 1998). Both isoforms are encoded by one single gene with alternative splicing (Langaese et al. 1997; Beesley et al. 2014). Np was discovered by utilizing a monoclonal antibody (mab) probe library to identify the glycoproteins enriched in synaptic structures (Hill et al. 1988; Hill et al. 1989). Interestingly, the intracellular carboxy-terminal tail of Np can exhibit variations through alternative splicing, leading to the emergence of variants including additional four amino acids: Asp-Asp-Glu-Pro

(DDEP) (Langnaese et al. 1997; Langnaese et al. 1998; Kreutz et al. 2001) (Fig.2). During development, Np55 expression is detectable at embryonic day (E) 14, and increases rapidly until postnatal day (P) 12, while Np65 is expressed postnatally (Hill et al. 1989; Langnaese et al. 1998).

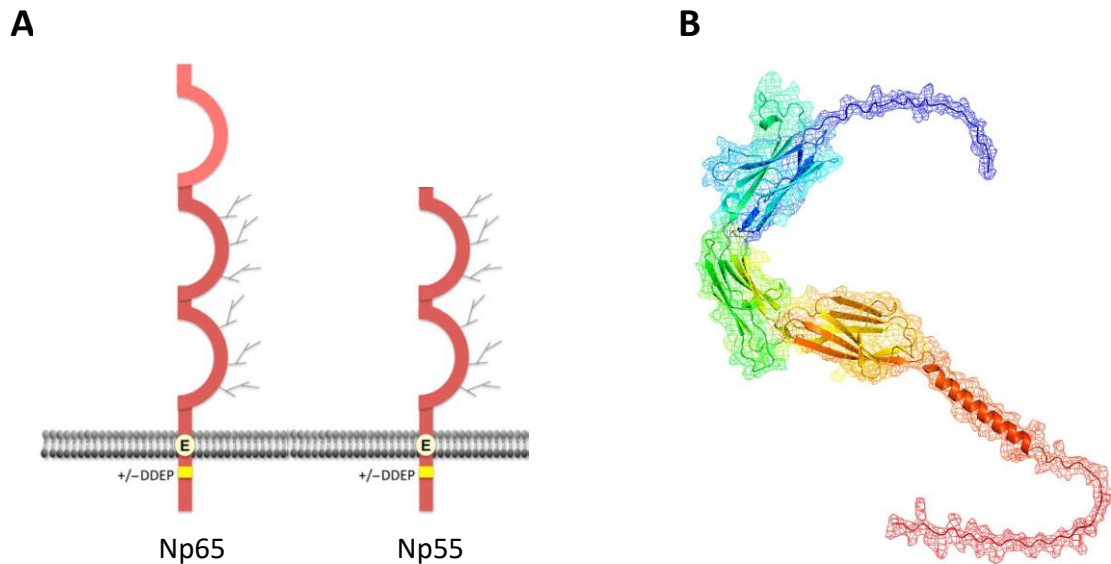


Figure 2: Schematic diagram of Np structures

A. Np55 contains two Ig domains and Np65 contains an extra domain at the N-terminal side, and the glycosylation sites are located in the second and third Ig domains. Alternative spliced isoforms lead to four extra amino acid (aa) (DDEP) in the cytoplasm. Figure modified from (Beesley et al. 2014). **B.** Schematic illustration of the protein structure prediction model of Np65 (Source: The PyMOL Molecular Graphics System, Version 1.2r3pre, Schrödinger, LLC.).

1.2.2. Molecular function of Np and binding partners

There are several molecular binding partners of Np. According to Jiang et al. (Jiang et al. 2021), the specific Igl of Np65 isoform interacts with AMPA receptor subunit GluA1, and it was described as crucial for Long Term Potentiation (LTP) maintenance. A function in spinogenesis was also reported for Np *via* binding to tumor necrosis factor receptor-associated factor 6 (TRAF6) (Vemula et al. 2020). Besides, Np65 was also reported to specifically colocalize with γ -Aminobutyric acid type A (GABA_A) receptor α 1 and α 2 subunits. This association is significant for the development of both excitatory and inhibitory synapses, which may play a crucial role in mediating cognitive

functions (Herrera-Molina et al. 2014; Amuti et al. 2016; Sarto-Jackson et al. 2012) (Fig.3).

Np65 isoform also shows trans-homophilic binding specifically between pre- and post-synapses, which could functionally be involved in p38 mitogen-activated protein kinases (p38MAPK) activation. A motif within the Ig2 module of Np55 was found binding to the fibroblast growth factor receptor1 (FGFR1), and the stimulation of FGFR1 may be involved in neuron outgrowth and synaptic plasticity (Owczarek et al. 2010). Moreover, Np was also found to serve as a crucial ancillary protein for the localization and activity of Monocarboxylate Transporter2 (MCT2) on the cell surface in some neuronal groups, and further plays a significant role in aiding the uptake of lactate for its utilization (Wilson et al. 2013). (Fig.3)

A very recently discovered binding partners of Np are the plasma membrane Ca^{2+} ATPases (PMCA) on which this dissertation focused.

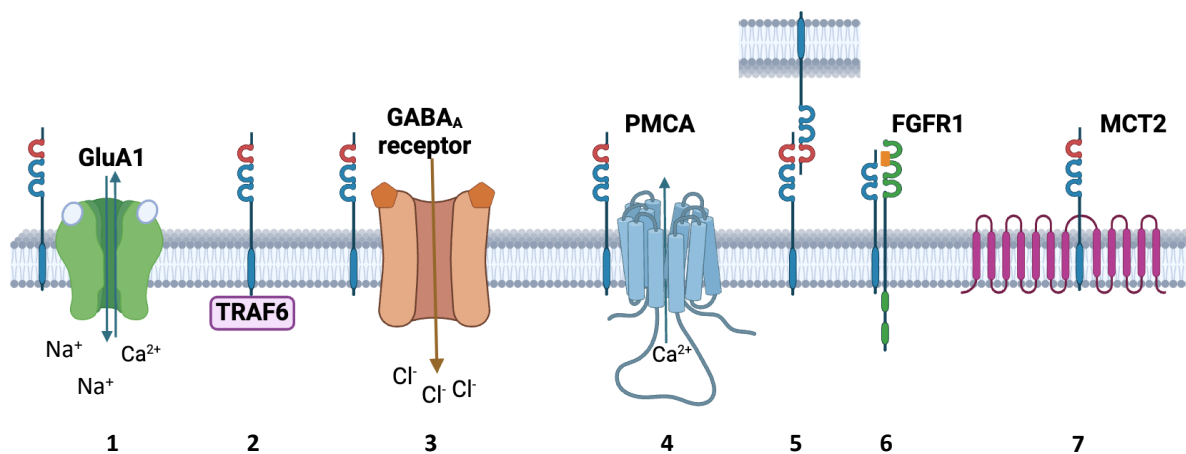


Figure 3: Schematic diagram of Np binding to different partner molecules

1. Igl of Np65 isoform interacts with AMPA receptor subunit GluA1. 2. Np binding with TRAF6 plays a role in spinogenesis. 3. Np65 interacts with GABA_A receptor further related to the formation of excitatory and inhibitory synapses. Np65 Interacts with $\alpha 1$, $\alpha 2$ and $\beta 2$ GABA_A receptor subunits. 4. Np binding with PMCA play roles in Ca^{2+} extrusion. 5. Trans-homophilic binding occurs between pre- and postsynaptic Np65 molecules. 6. Interaction between Np55 and FGFR1 involves the two middle Ig domains. 7. Np directly binds to and facilitates MCT2 function, playing a significant role in promoting the uptake of lactate utilization. (Figure modified from biorender.com)

1.3. Plasma membrane Ca^{2+} ATPases (PMCA)

1.3.1. PMCA and Np

There are four different genes *ATP2B1-4* encoding plasma membrane Ca^{2+} ATPases (PMCA1-4) as the major system for calcium extrusion expressed in mammalian cells. Among them, PMCA1 and PMCA4 are the universal variants found in almost all tissues, whereas PMCA2 and PMCA3 have a more limited distribution such as in nervous and muscle tissue (Brandt et al. 1992; Zacharias et al. 1999; Jensen et al. 2007; Boczek et al. 2021). Besides, PMCA2 is also highly expressed in cochlear outer hair cells (OHCs) and spiral ganglion cells (SGN) (Lin et al. 2021a; Newton et al. 2022). Numerous studies have shown that Ca^{2+} is crucial in regulating neuronal plasticity, which is fundamental to learning, memory, and neuronal survival. Both intra- and intercellular mechanisms control Ca^{2+} homeostasis in the brain, ensuring proper neural function and preserving neural integrity. As one of the three most important main calcium pumps, PMCA plays crucial roles along with sarco/endoplasmic reticulum Ca^{2+} -ATPase (SERCA) and secretory pathway Ca^{2+} -ATPase (SPCA) in contribution to neuronal Ca^{2+} homeostasis (Boczek et al. 2021).

So far, it has been clearly proven that the protein levels and stabilization of the four PMCA paralogs strongly depend on the binding to and the formation of protein complexes with Np. Loss of Np strongly reduced the protein but not mRNA level of PMCAs in mouse (Herrera-Molina et al. 2017; Korthals et al. 2017). Np plays a critical role for the effective trafficking of PMCA and the efficient control of PMCA-mediated Ca^{2+} clearance. By interacting with PMCA, Np could influence the spatial distribution of PMCA pumps, further targeting PMCA to the membrane regions of high Ca^{2+} influx where efficient clearance is required (Herrera-Molina et al. 2017; Schmidt et al. 2017; Gong et al. 2018). Experiments already showed that the expression level of PMCA could be promoted by exogenous Np and accelerated Ca^{2+} extrusion from cytoplasm which ensures the fast restoration of the basal level following neuronal excitation (Malci et al. 2022).

1.3.2. Np related diseases

In addition to the above-mentioned messages that the *NPTN* gene might be one of the genetic factors contributing to cortical layer thickness changes in adolescents

and schizophrenia, there are also several studies reporting possible pathogenicity of Np proteins in human or animal models.

Research using proteomic identification showed Np over-expression could lead to a significant increase in breast cancer tumor growth and angiogenesis (Rodriguez-Pinto et al. 2009). Researchers from Japan investigated the level of Np which is highly expressed in lung cancer cell. Activation of the NFI transcription factors NFIA, NFIB and SAM pointed-domain, eventually leads to the aggressive phenotype appearance (Sumardika et al. 2019). Besides, immunohistochemical analyses were performed by Ilic et al. on tissues from human Alzheimer's disease (AD) patients. By comparing with the age-/gender-matched control subjects, the expression level of Np65 in AD patients in the dentate gyrus (DG), cornu ammonis 2/3 (CA2/3), and subiculum was significantly increased, and also depended on the progress of the disease (Ilic et al. 2019).

With different transgenic mice, such as complete knockout Np (Bhattacharya et al. 2017), specific knockout of Np65 (Amuti et al. 2016), conditional knockout of Np in glutamatergic neurons (Herrera-Molina et al. 2017) and also inducible loss of Np in neurons (Bhattacharya et al. 2017), lack of Np was shown to lead to learning and memory deficits, anxiety, and depression-like behavior in mice (Bhattacharya et al. 2017; Li et al. 2019). Moreover, Np was also found to be involved in aging and chronic stress in rats (Balog et al. 2022).

1.3.3. PMCA related diseases

Researches on the relationship between PMCA and neuropathologic diseases have been reported. Firstly, it was found that PMCA activity and abundance are progressively decreasing along with the age (Michaelis et al. 1984; Michaelis 1989; Michaelis et al. 1996). In AD patients, the presence of amyloid β -peptide ($A\beta$) plaques, a crucial histological biomarker, is associated with the abnormal accumulation of tau protein. Related studies have revealed that $A\beta$ could decrease the activity of purified PMCA and especially present the inhibition for the isoform PMCA4 (Mata et al. 2011; Berrocal et al. 2015).

Studies about schizophrenia demonstrated that kinetic properties of calmodulin (CaM)-stimulated PMCA were altered in patients (Kluge et al. 1985). A further global proteomic analysis from schizophrenia patients and a control group indicated that

upregulated PMCA4 could be one of the reasons mediating the abnormal brain Ca^{2+} homeostasis (Martins-de-Souza et al. 2009).

Additionally, isoforms PMCA2 and PMCA3 are highly expressed in mouse cerebellum and forebrain. It has been proven that PMCA2 knock out mice exhibited severe cerebellar ataxia, and several mutations from PMCA2 and PMCA3 all lead to the prolonged duration of Ca^{2+} transients and deficits to maintain Ca^{2+} homeostasis in neurons (Boczek et al. 2021). Evidence also converged to support an association between *ATP2B2* gene variants and autism (Carayol et al. 2011).

1.3.4. Np and PMCA function in the hearing system

One of the very interesting points about the possible pathogenicity of both Np and PMCA alterations is the role they play in the hearing system, which was also the starting point for the conduct of this research.

The structural and functional integrity of the mammalian inner ear play important roles in maintaining a fully functional hearing. There are two types of hair cells in the cochlea, the outer hair cells (OHC) and the inner hair cells (IHC) (Fig.4A). The number of OHCs is three to four times larger than of IHCs. OHCs mechanically amplify the sound-induced vibrations, while the IHCs activate the auditory nerve *via* ribbon synapses on spiral ganglion neurons (SGNs). (Elliott et al. 2012; Raphael et al. 2003) Np55 is strongly expressed in the stereocilia of OHCs and in the cell bodies of IHCs, whereas the expression of Np65 in the cochlea is inconclusive (Zeng et al. 2016; Lin et al. 2021a; Newton et al. 2022). Besides, the PMCA2 isoform is especially concentrated in the hair bundles of OHCs, and the PMCA1 isoform distributes in the basolateral membrane of IHCs (Lin et al. 2021a; Newton et al. 2022; Fettiplace et al. 2019; Driver et al. 2020) (Fig.4B).

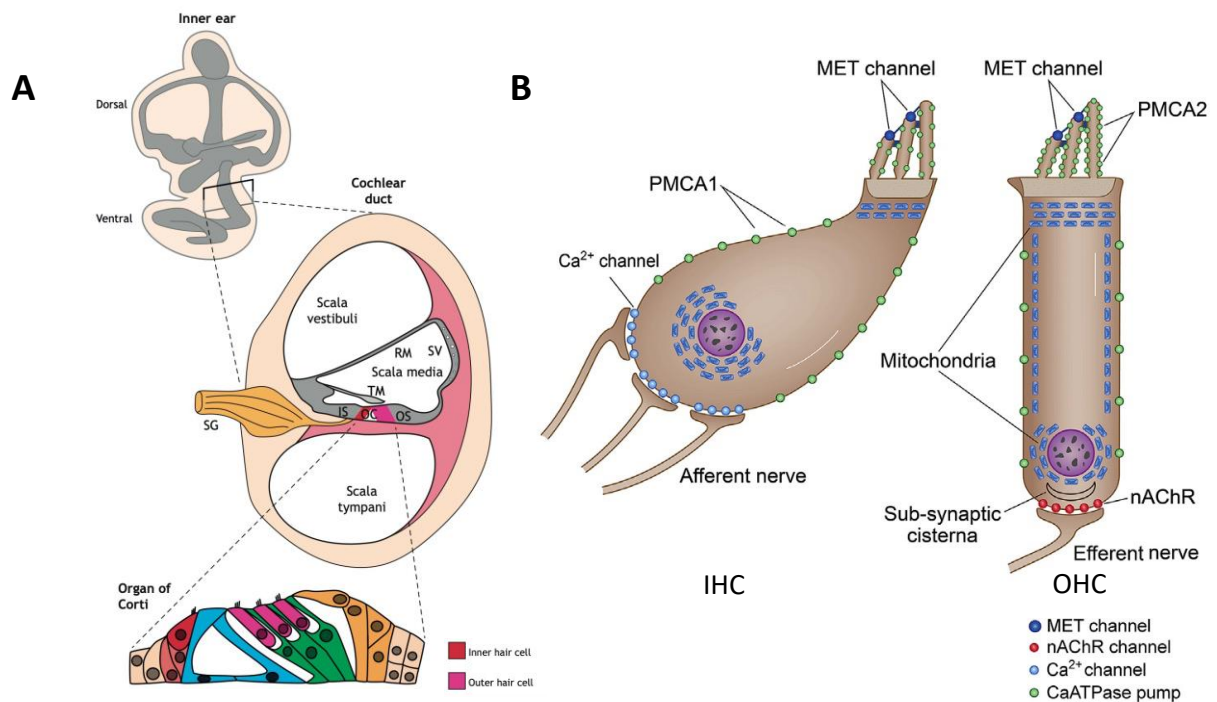


Figure 4: Schematic illustration of the structure of the inner ear and Ca^{2+} homeostasis in hair cells

A. The inner ear structure is composed of the vestibular system and the cochlea. Within the cochlea, the cochlear duct is divided into three chambers: the scala vestibuli, scala media, and scala tympani. The scala media houses the organ of Corti (OC) and contains both OHCs and IHCs. These hair cells possess hair bundles that make contact with the tectorial membrane (TM). The auditory signals detected by the inner hair cells are transmitted to the central nervous system (CNS) through the bipolar neurons located in the spiral ganglion (SG).

B. PMCA1 primarily facilitates the expulsion of Ca^{2+} from the soma of IHCs. Meanwhile, PMCA2 is notably abundant in OHCs, and responsible for extruding Ca^{2+} from the stereocilia. Figures modified from (Driver et al. 2020; Fettiplace et al., 2019).

Recently, Np was identified as a crucial protein for deafness. Two by N-ethyl-N-nitrosourea (ENU) mutagenesis generated mice *pitch* and *audio-1* were reported (Carrott et al. 2016; Zeng et al. 2016). The expression of Np in these mutants was decreased because of the truncated and/or instable and further lead to the impairment in hearing ability. Besides, Lin et al. reported that mice in both Np congenital knock out (*Np^{kn}*) and induced-Np loss in adult neurons after normal development all led to the deafness (Lin et al. 2021a)

In addition, these studies also noted that the lack of Np led to a reduction in PMCA1 in the IHCs and complete absence of PMCA2 in the stereocilia of OHCs in adult *Nptn*^{-/-} mice (Lin et al. 2021a; Newton et al. 2022). In cochlear OHCs and spiral ganglia, PMCA2 is highly expressed (Fettiplace et al. 2019). Furthermore, deletion or mutations in *Atp2b2* and *ATP2B2* encoding PMCA2 result in hearing loss and also cognitive deficiencies in mice and humans (Kozel 1998; Schultz et al. 2005; Bortolozzi et al. 2018).

So far, missense mutations in *Nptn* leading to hearing impairment were only detected in mice (Carrott et al. 2016; Zeng et al. 2016; Lin et al. 2021a). The molecular mechanism of hearing impairment due to dysregulation of the interaction between Np and PMCA2 is unknown. Currently it is also not known whether *pitch* and *audio-1* mice display cognitive deficiencies comparable to *Nptn*^{-/-} (Carrott et al. 2016; Zeng et al. 2016). In addition, only mutations in the *ATP2B2* gene have been described to cause abnormalities of hearing or NDDs in human. Diseases caused by mutations in the *NPTN* gene and the related pathogenesis in human have not been described.

1.4. Np's homology in *Drosophila*-Basigin

Basigin (Bsg) is the only *D. melanogaster* member of the Basigin/Embigin/Neuroplastin subfamily within the Immunoglobulin superfamily (IgSF). Bsg shares a high degree of similarity with Np in the regions encompassing and adjacent to the transmembrane sequence, including the charged glutamate residue, and within the intracellular domains (Langnaese et al. 1997; Munro et al. 2010). The residue mutated hNp^{p.P342L} variant (p.P>L in *Drosophila*) in this study is just located in the transmembrane domain (TM) (Fig.5). Additionally, Bsg has been identified plays a key role in the formation of neuromuscular junction (NMJ) in fruit flies by mediating the interactions between pre- and post-synapses (Besse et al. 2007). Therefore, using the NMJ as a genetic model is a good choice to study the expression level and functionality of mutated hNp in an *in vivo* system.

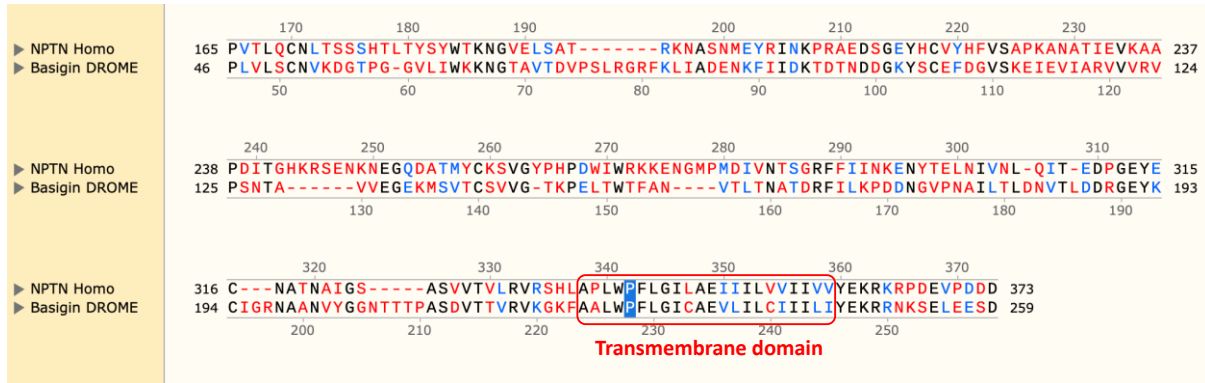


Figure 5: Sequence alignment of Np in human and Bsg in *Drosophila*

Identical residues are marked in black, similar residues are marked in blue and non-similar residues are marked in red. The highly homologous transmembrane area is in the red frame, and the p.P>L mutation mentioned in this research is noted in blue background.

2. Hypothesis and aims of the thesis

The underlying hypothesis proposes that mutations in *NPTN* are pivotal in the pathogenesis of NDDs and auditory dysfunctions by disrupting PMCA function, thereby impairing Ca^{2+} signaling. To investigate this, the study aims to analyze the impact of these variants on Np and PMCA expression levels in HEK293T cells and primary hippocampal neurons and to examine the effects on Ca^{2+} extrusion under different expression conditions. Finally, expression of a pathogenic *NPTN* variant in a transgenic *Drosophila* model shall prove that the mutation is causal for PMCA malfunctions *in vivo*. Through the multifaceted approaches, the molecular mechanisms by *NPTN* mutations contribute to NDDs shall be investigated.

3. Materials and Methods

3.1. Generation of constructs encoding WT and Mutated Np

3.1.1. Primer design

Human Np55 and Np65 (hNp) cDNA containing constructs were obtained from GenScript (Piscataway, NJ; Clone IDs: OHu06230D). PMCA2-GFP construct was bought from Addgene (Watertown, MA). TagRFPT-GCamp5 and Gcamp7 constructs have been described by Malci et al. 2022. Mutations were introduced into cDNA plasmids by PCR amplification using the following primers from Biomers (Ulm, Germany):

Table 1: Primer list for all constructs

Constructs	Primer sequence
hUbC-forward	5'-CTGAAGCTCCGGTTTTGAAC-3'
FUGW_vorLTR- reverse	5'-CGTTGGGAGTGAATTAGCC-3'
hNp55/65WT FUGW-forward	5'- GACTCTAGAGGATCCAGGATGTCGGGTTTCGTCGC TGCC -3'
hNp55/65WT FUGW-reverse	5'- GTTTTTCTAGGTCTCGAGTTAATTTGTGTTTCTCTGGCGC-3'
hNP55_65-C200-316S-forward	5'-GGCGAGTATGAAAGTAATGCCACCAAC-3'
hNP55_65-C200-316S-reverse	5'-GTTGGTGGCATTACTTTCATACTCGCC-3'
hNP55-second_I34N-forward (extra-long)	5'-GTCACCAGTGAAGAGGTCATTATTCGAGACAGCCCT-3'
hNP65-I150N-forward	5'- CAGAAGCCAAGGAATGTCACCAGTGAA-3'
hNP65-I150N-reverse	5'- TTCACTGGTGACATTCCTTGGCTTCTG-3'
hNP65-W135R-forward	5'- CCC TCC ATA ACA AGG ATT CGA GCC CAG GCC ACC-3'
hNP65-W135R-reverse	5'- GGT GGC CTG GGC TCG AAT CCT TGT TAT GGA GGG-3'
hNp65T194P-forward	5'-- GAACTGAGTGCCCCTCGTAAGAATGCC 3'
hNp65T194P-reverse	5'- GGCATTCTTACGAGGGGCACTCAGTTC -3'

hNP55/65-P226/342L- forward	5'- GCCCCACTCTGGCTTTTCTTGGGAATT-3'
hNP55/65-P226/342L- reverse	5'- AATTCCCAAGAAAAGCCAGAGTGGGGC-3'
RFPT-GCaMP5-forward	5'-ACTCTAGAGGATCCAGGATGGTGTCTAAGGGCGA-3'
RFPT-GCaMP5-reverse	5'-CATGTTTTTCTAGGTCTCGAGTCACTTCGCTGTCATC-3'
cf_pJFRC12_hNp55- forward	5'- CTAGGCGGCCGCGGCTCGAGAATCAAATGTCGGGTTTCG TCGCTG -3'
cf_pJFRC12_hNp55_ST OP-reverse	5'- CTTCACAAAGATCCTCTAGATTAATTTGTGTTTCTCTGGCG C-3'

3.1.2. Polymerase Chain Reaction (PCR)

Amplification of DNA fragments was performed with the following reaction mixture and program:

Table 2: Reagents and volumes for PCR

Reagents	Volumes
Template DNA (20-50 ng)	1 µl
5X HF buffer	10 µl
dNTPs 10mM (Invitrogen)	1 µl
Phusion polymerase (Thermo Scientific)	0.2 µl
Forward primer (Biomers)	0.2 µl
Reverse primer (Biomers)	0.2 µl
ddH ₂ O	37.4 µl
In total	50 µl

Table 3: PCR amplification program

Initial denaturation	95°C	5'	
Denaturation	95°C	45"	
Annealing	60°C	30"	32-35 cycles
Elongation	70°C	60"	
Final elongation	72°C	10'	

The PCR products were separated by 1% agarose gel electrophoresis then cut out from the gel under UV-light and purified using Nucleo Spin Gel and PCR clean up kit (Macherey-Nagel).

Table 4: Reagents for agarose gel electrophoresis

Reagents	Composition
Agarose (Biozyme LE) Molecular biology grade	0.7 to 2%
50x TAE	2 M Tris, 0.05 M EDTA, 1 M Acetic acid
Ethidium Bromide (Roth)	1% stock solution
6x Loading Dye (Fermentas)	10 mM Tris-HCl (pH 7.6), 0.03% bromophenol blue, 0.03% Xylene cyanole FF, 60% glycerol, 60 mM EDTA
1kb DNA Smart ladder (Biolabs)	Gel Loading Dye, Purple (6X), no SDS

3.1.3. Cold Fusion™-based cloning procedure

The cold fusion technology is a simple, rapid and highly efficient PCR-product cloning kit. It was used to directly ligate the PCR products with the linearized FUGW expression vector (all gel-purified). Linearized FUGW vector was generated by double restriction digestion with BamHI (Fermentas) and XhoI (Fermentas). The PCR products were mixed as below. The reaction mix was incubated at room temperature (RT) for 5 min followed by 10 min on ice.

Table 5: Reagents for Cold fusion cloning procedure

Reagents	Volumes
Linearized destination vector (10-100ng/ μ l)	2 μ l
PCR insert(s)	2.5 μ l
5x Master Mix (Cold Fusion Cloning Kits, BioCat)	2 μ l
ddH ₂ O	adjust to 10 μ l

3.1.4. Transformation of bacteria

For the transformation of E. coli XL10-GOLD (from Dr. U. Thomas), 10 μ l of the cold fusion reaction were incubated with 50 μ l bacteria on ice for 20 min. After a 50-second heat shock at 42°C, the mixture was incubated on ice for 2 min. Then 250 μ l Lysogeny broth (LB) Medium were added and the transformed bacteria were incubated at 37°C for 1h with shaking at 400rpm constant speed and then plated on LB-agar plates with respective antibiotics (pre-warmed at RT). The plates were incubated overnight at 37°C.

3.1.5. Mini preparation and restriction digestion

The Mini-Prep procedure is used to isolate small amounts of plasmid DNA from bacteria for restriction analysis, sequencing and cloning. Bacteria are grown in 2ml LB medium (with antibiotics) overnight, harvested and the DNA is purified according to the QIAprep® Miniprep Handbook. Restriction digests were performed as indicated below at 37 °C for 1 hour. Finally, the results of the digest were visualized after agarose gel electrophoresis.

Table 6: Reagents for Restriction Digestion

Reagents	Volume
DNA construct	10 μ l
Cut smart buffer	2 μ l
BamHI	0.2 μ l
XhoI	0.2 μ l
ddH ₂ O	adj 20 μ l

3.1.6. Plasmid Midi preparation

Single bacterial colonies were used to inoculate cultures in LB medium with corresponding antibiotic overnight. Then plasmid DNA was prepared by using Xtra Midi EF Kit (Macherey-Nagel) according to the manufacturer's instructions.

3.2. Human Embryonic Kidney (HEK)293T cell culture

HEK293T cells were maintained as recommended by ATCC (<https://www.atcc.org/products/crl-3216>).

Table 7: Medium list in HEK293T cell culture

Base medium	Dulbecco's Modified Eagle's Medium (DMEM)
Complete growth medium	10% Fetal Bovine Serum (heat inactivated), 1% penicillin and streptomycin and 1% L-glutamine

3.2.1. Transfection of HEK293T cells

Cultures were transiently transfected with the plasmids (1.5 µg DNA/well for WB, 0.5 µg DNA/well for IHC) by mixing with Lipofectamine 2000 (#11668-019, Invitrogen) (for 6-well plates, 3 µl per well, for 12 well plates, 1 µl per well).

Transfection was done 24 hours after seeding and harvested for staining or Western blot analysis 24 hours later.

For protein degradation inhibitor treatment, HEK293T cells were subjected to a treatment with either MG132 (5 µM) or ammonium chloride (50 mM) 16-hour post-transfection. Cell harvesting was performed 6 hours after the treatment.

N-linked oligosaccharides were enzymatically digested using PNGaseF (New England Biolabs, Frankfurt am Main, Germany) under denaturing conditions. A total reaction volume of 10 µl was prepared by combining 20 µg of glycoprotein with 1 µl of denaturing buffer (10x), followed by heating at 100°C for 10 minutes. After addition of 2 µl Glycobuffer2 (10x), 2 µl 10% NP40, 6 µl H₂O, and 1 µl PNGaseF, the reaction mix was incubated at 37°C for 1 h and then assessed on SDS-PAGE gels.

3.2.2. Measurement of protein concentration by Amido Black

200 µl Amido Black was added to 2µl test samples and incubated for at least 20 min at RT with shaking. Samples were then centrifuged at 14000 rpm at RT for 5 min, the pellet was resuspended in 1 ml wash solution, spun again and the procedure was repeated at least 3 times until the buffer appeared colorless. The last pellet was air-dried and dissolved in 300 µl 0.1 M NaOH and the OD was measured at 620 nm.

Table 8: Wash solution and Amido Black solution recipe

Wash solution	900 ml methanol, 100 ml acetic acid
Amido Black solution	14.4 g Amido Black, 1 l wash solution

3.3. Western Blot

HEK293T cells were harvested with lysis buffer and then homogenized by using an ultrasonic homogenizer. Then centrifuged at 14000 rpm at 4°C for 10 min. The supernatant was collected and mixed uniformly with 2xSDS loading buffer and boiled at 95°C for 15 mins. Proteins were separated by sodium dodecyl sulfate–polyacrylamide gel electrophoresis (SDS-PAGE) on 10% gels and transferred to a nitrocellulose membrane (Whatman). After blocking by non-fat milk (5%) for 1h, the membrane was incubated with primary antibodies (sheep anti-Np; mouse anti-GFP, mouse anti- β-actin) overnight at 4°C. After washing the membrane 3 times (10mins each time) by using 1xTBST, the blots were incubated with secondary antibodies for 1h at RT. After washing, the membrane was incubated with ECL buffer and chemiluminescence was detected.

Table 9: Western Blot buffer list

Buffer	Composition
Lysis buffer	150 mM NaCl, 1% Ecosurf™ EH-9, 50 mM Tris-HCl (pH 8.0) +Protease Inhibitor Cocktail
2x SDS buffer	125 mM Tris-HCl, pH6.8, 4% SDS, 20% glycerin, 0.2% bromophenol blue, 10% β-mercaptoethanol, ddH ₂ O
10x TGS buffer	Bio-Rad (161-0772)
10x Blotting buffer	0.25 M Tris-base, 1.92 M glycine, 0.2% SDS, ddH ₂ O
1x Blotting buffer	10x blot buffer, methanol, ddH ₂ O
Ponceau S	0.5% Ponceau S, 3% TCA, ddH ₂ O
10x TBS	0.2 M Tris-base, 1.37 M NaCl, ddH ₂ O, pH 7.6
1x TBS	10x TBS, ddH ₂ O
1x TBS-T	10x TBS, Tween-20, ddH ₂ O
1x TBS-A	10x TBS, 5% Sodium Azide, ddH ₂ O
ECL buffer	WBKLS0500, Merck, Darmstadt, Germany

3.4. Total RNA isolation and qPCR

Total RNA was isolated from HEK293T cells transfected with hNP WT/variants 24 hours after transfection using the RNeasy Plus Mini Kit (Qiagen). The concentration of RNA was determined by 260nm absorbance *via* Nanodrop 1000. 200ng of total RNA was used for cDNA synthesis using the RT2 First Strand Kit (Qiagen). The detectors of human Np (Hs01033353_m1, Thermo Fisher) and human GAPDH (Hs02758991-g1, Thermo Fisher) TaqMan gene expression assays were arranged in 96-well plates and cDNA from each hNp genotype duplicated for 3 wells. Quantitative real-time PCR amplification program was as follows: 50°C 2mins hold, 95°C 10mins hold for activation of the polymerase, followed by 45 cycles with 15 secs at 95°C and a hold for 60°C 1min. Relative quantification was performed with the 7300 real-time PCR system (Applied Biosystems).

3.5. Culture of hippocampal neurons

Cultures of hippocampal neurons were prepared as described previously (Herrera-Molina R, et al., 2014) with modifications from Sprague-Dawley rat embryo day 18 (E18). Brains were carefully removed, collected in cold HBSS⁻, and the hippocampus was dissected under a stereo microscope. The hippocampus was placed in a small Petri dish in cold HBSS⁻ and then washed 3-5 times with HBSS⁻ in a 15ml Falcon tube. Then, the tissue was dissociated with 0.25% Trypsin for 20 min at 37°C in a water bath. Trypsin was removed by washing the hippocampus 4-5 times with 10ml HBSS⁻. After the final washing, 1.6ml HBSS⁻ and 400 µl 0.05% DNaseI solution was added. The hippocampus was transferred to an Eppendorf cup and cells were dissociated by passing the suspension through two different sized needles (3x0.9mm needle, 3x0.5mm needle), or alternatively a fire polished Pasteur pipette was used. The cell suspension was filtered through nylon gauze (125µm pore size) to remove debris and then diluted with 20ml plating medium (DMEM+). In each well of 12-well plates, 50.000 neurons were seeded in 1 ml of medium. One hour following seeding, the initial culture media was substituted with 1 ml of Neurobasal medium, which was enriched with 1% B-27 supplement, 1% penicillin/streptomycin, and 1% L-glutamine. On the 7th day, either 100µl or 200µl of complete medium was added.

3.6. Transfection of hippocampal neurons

Hippocampal neuron cultures were transiently transfected with plasmids (for 12 well plates, 0.5 µg per well) after mixing with Lipofectamine 2000 (for 12 wells, 1 µl per well). Transfection was done at Day *in vitro* (DIV) 11 and cells were fixed for staining 48 hours after transfection. *In vitro* neuron Ca²⁺ imaging was performed on DIV14.

3.7. Immunocytochemistry in hippocampal neurons

Rat hippocampal neurons were co-transfected with either hNp55/65^{WT}, or hNp variants and GFP plasmids at DIV11, then were fixed and stained for Np and PMCA according to the protocol established in the lab (Lin, et al., 2021a; Herrera-Molina et.al., 2017). Cells were fixed by incubation of the coverslips with 4% paraformaldehyde (PFA) with extra 2-4% sucrose for 8-10 minutes and then washed briefly with 3x PBS. Permeabilized and blocked in PBS with 10% horse serum and 0.1% Triton X-100 for

40 minutes at room temperature. Then incubated with the blocking solution with primary antibodies (sheep anti-Np; mouse anti-PMCA) overnight at 4°C in the ratio of 1:500 mixed with blocking buffer. After incubation, the coverslips were washed with 1x PBS for 3 times for 10 minutes each. Secondary antibodies (donkey anti-sheep cy3, donkey anti-mouse cy5; Jackson ImmunoResearch, Ely United Kingdom) were mixed in the blocking solution in the ratio of 1:1000, added to the coverslips and incubated in RT for 1h. The coverslips were then washed with 1x PBS for 3 times and fixed on microscopy slides with Mowiol.

Table 10: Immunocytochemistry buffer list

Reagents/Solutions	Composition
4% PFA	40g Paraformaldehyde, 1L 1xPBS (add 1 M NaOH and stir gently on a heating block at ~60°C until the paraformaldehyde is dissolved.)
10xPBS	1.37 M NaCl, 27 mM KCl, 100 mM Na ₂ HPO ₄ , and 18 mM KH ₂ PO ₄
Blocking buffer	1xPBS with 10% Horse serum (with/without 0.05% Triton-X100)
Mowiol	2.4g Mowiol, 6g Glycerol, 6ml distilled water and 12 ml 0.2M Tris-HCl (pH 8.5)
PBS-DAPI	1µg/ml of 1xPBS

3.8. Calcium live imaging

Rat hippocampal neurons were co-transfected with either hNp55/65^{WT}, or hNp variants and RFPT- GCamP5 plasmids at DIV11. Ca²⁺ imaging was performed at DIV14-16. The coverslips were inserted into an imaging magnetic chamber (Warner Instruments, Hamden, CT, USA) with recording buffer. The neurons were electrically stimulated with 10 pulses at 10/20/100 Hz generated by a S48 stimulator (Astro-Med, Inc., West Warwick, RI, USA), and this process was recorded by an inverted microscope (Observer. D1; Zeiss, Jena, Germany) combined with an EMCCD camera (Evolve 512; Delar Photometrics, Tucson, AZ, USA) under VisiView® Software (Visitron Systems GmbH, Puchheim, Germany) at 63x 1.2 N.A magnification.

For data analysis, the images were first quantified using Fiji ImageJ. 3-4 dendrites from each neuron were selected as regions of interest (ROI) and then the curves were generated using Clampfit (version 10, Molecular devices, San Francisco, CA, USA) and the decay time, peak amplitude and halfwidth were calculated.

Table 11: Calcium imaging buffer list

2 x Tyrodes buffer	5 mM KCl, 50 mM HEPES, 60 mM glucose
Recording buffer	119 mM NaCl, 1x Tyrodes buffer, 2 mM MgCl ₂ and CaCl ₂ , ddH ₂ O

3.9. Generating transgenic flies for expression of hNp55^{p.P>L}

The UAS-hNp55 transgenic constructs described in chapter 3.1 were used for PhiC31-mediated germ line transformation into the attP40 target site on the second chromosome (cytological position 25C6) of the recipient strain (genotype: $y^1 w^{67c23}; P$ [CarryP] attP40) (Bateman et al. 2006). This procedure was performed at BestGene (Chino Hills, CA). Transgenic flies were identified based on orange eye color and established as stocks carrying the *CyO^{GFP}* balancer chromosome. Next to balancer-carrying heterozygotes also homozygous transgenic flies are present in the strain.

3.10. Recombination of transgenic lines and Gal4-induced expression.

In order to perform rescue experiments, transgenic flies carrying both a Gal4-inducible UAS-bsg-RNAi construct (on third chromosome) and either the Gal4-inducible UAS-hNp55 or UAS-hNp55^{p.P>L} construct, recombinant strains were established, taking advantage of traceable dominant markers associated with balancer chromosomes.

In the end, the *Drosophila* stocks are as follow: Control w1118, Bsg RNAi^{GD2789}, Bsg RNAi^{GD2789}+ hNp55^{WT} Rescue, Bsg RNAi^{GD2789}+ hNp55^{p.P>L} Rescue, C57-Gal4.

The recombined *Drosophila* lines generated according to the following work flow as follows:

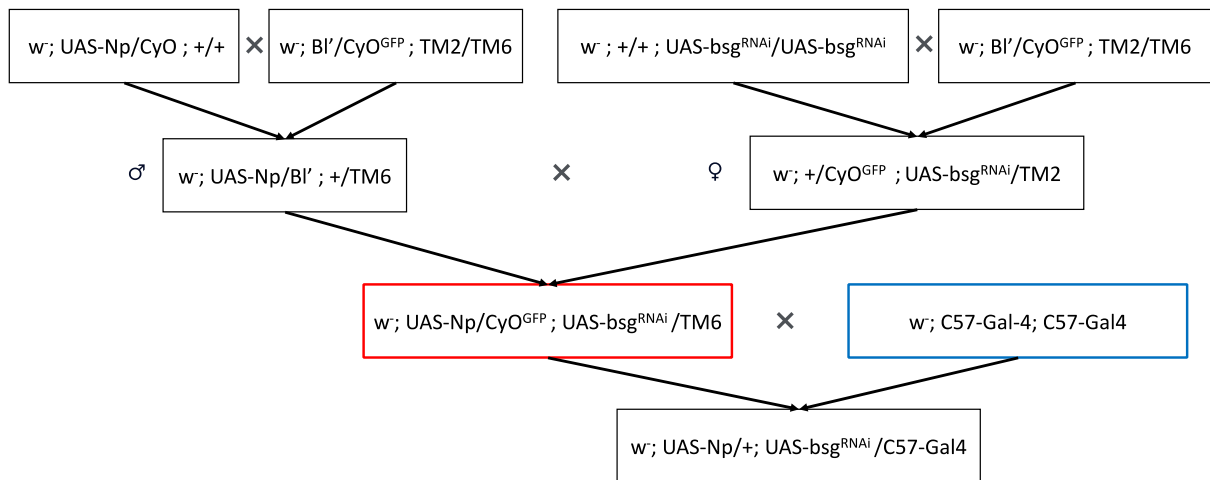


Figure 6: Generation of recombined *Drosophila* lines for Gal4-induced co-expression of bsg-RNAi and hNp55

Only the second and third chromosomal genotypes are depicted, separated by semicolon. Marker and balancer chromosomes include Bl^1 (recognizable as shortened bristles), CyO^{GFP} (recognizable by green fluorescence and by curled wings), TM2 (recognizable by swollen halteres) and TM6 (recognizable by tubby appearance during larval/pupal stages and by super nummary bristles in the humeral part of the adult thorax). Segregations of these markers was used as a criterion to select flies with the desired genotypes. The $UAS-hNp55^{(WT \text{ or } p.P>L)}/CyO^{GFP}; UAS-bsg-RNAi/TM6$ recombinant flies (red box) were established as a stable stock, from which males or females were crossed to the muscle-specific Gal4-activator line *C57-Gal4* (blue box).

3.11. Immunohistochemistry in larvae

Larvae were dissected in Ca^{2+} free dissection buffer (128 mM NaCl, 36 mM sucrose, 2 mM KCl, 1 mM EGTA, 5 mM HEPES, 4 mM $MgCl_2$) in a dissecting chamber using microdissection scissors, forceps and magnetic pins (Marter et al. 2019). Fixation was done by exchanging the dissecting buffer with 4% PFA in 0.1 M phosphate buffer and subsequent incubation for 20min at RT. The fixative was then removed by quickly rinsing 3 times in 0.1 M PB with 0.2% Triton X-100 (PBT), followed by two more changes over 20 min. Fixed samples were incubated with primary antibodies (sheep anti-Np, RD systems; rabbit anti-PMCA, from Dr. U. Thomas) overnight at 4 °C in the ratio of 1:300 in PBT. After incubation, the larvae were washed with 1x PBT for 3 times for 10 min each. Secondary antibodies (donkey anti-sheep Cy3, donkey anti-rabbit Alexa488 and goat anti-Hrp 647; Jackson ImmunoResearch) were then mixed in the

PBT in the ratio of 1:300, added to the well and incubated for 1 hour in RT. Samples were then washed again with PBT 3 times for 10 min and mounted on microscopy slides with Vectorshield (Vector Laboratories, Newark, CA).

3.12. Confocal microscopy

Images were captured using the HCXAPO X 63/1.40 NA oil immersion objective on an upright Leica TCS SP5 confocal microscope, utilizing the sequential scanning mode and a Pinhole setting of 1 Airy Units (AU). Rat hippocampal neuron images were collected at a resolution of 512 X 512 pixels at 200 Hz, applying magnifications of 3-fold. *Drosophila* NMJs images were captured at a resolution of 1024X 512 pixels with 2.5-fold zoom factor. The z- step size was 0.3 nm. In each larva, 2-3 NMJs from both left and right side of A2 or A3 body wall segment were selected.

Analysis of PMCA and Np in rat hippocampal neurons were quantified by using Fiji. 6-8 equal length short lines (2 μ m) were selected from each neuron to do the line scan analysis. The middle point of the lines located in the soma membrane. The plot profile function was used to display a two-dimensional graph of the intensity of pixels along the line. Analysis of PMCA in larvae NMJs were performed by manually using maximum intensity and Z-projection method of Fiji. Firstly, Z-stacks images were projected as "Max Intensity". Hrp signal channel threshold was adjusted with 2-pixel median filter. Then obtained the ROI after apply the "Otsu" threshold setting. For PMCA channel, edited the extra selection area in 3 pixels enlargement setting, then got the final interested area generated by the XOR ('Exclusive OR').

3.13. Statistical analysis

Statistical analysis of data was performed using Prism9 software (GraphPad), with outliers from raw data screened out with the Grubbs' test (Q=1). For Western blots and Immunocytochemistry, statistical analysis of optical density measurement data used Student's t-test. For Ca²⁺ imaging, a Mann-Whitney U test was used for group comparisons for non-parametric data with sample sizes > 20, and a Wilcoxon matched pairs test for the inner group comparison. A P-value of ≤ 0.05 was considered significant. p ≥ 0.05 was labeled as "ns"; * indicates p < 0.05; ** indicates p < 0.01; *** indicates p < 0.001; **** indicates p < 0.0001. All values are shown as mean \pm standard error of the mean (SEM).

4. Results

4.1. Generation of plasmids for the expression of mutated human Np

Five human *NPTN* variants were investigated in this study. Two variants correspond to the previously identified *pitch* and *audio-1* mouse mutants which developed deafness transferred into human cDNA background: c. 449T>A p. Ile150Asn (*audio-1*), c. 946T>A p. Cys316Ser (*pitch*) (Carrott et al. 2016; Zeng et al. 2016). Furthermore, three *NPTN* variants from human patients with *de novo* missense mutations were reported: c.403T>A, p. Trp135Arg (p.W135R); c. 580A>C p. Thr194Pro (p.T194P), c.1025C>T p. Pro342Leu (p.P342L). Of those variants, p.T194P was also identified in unaffected population controls (gnomAD, v4.0.0) (Fig.7A). Comparison of human, mouse, and rat Np amino acidic sequences shows that Np is highly conserved between the species at the mutation sites (Fig.7B).

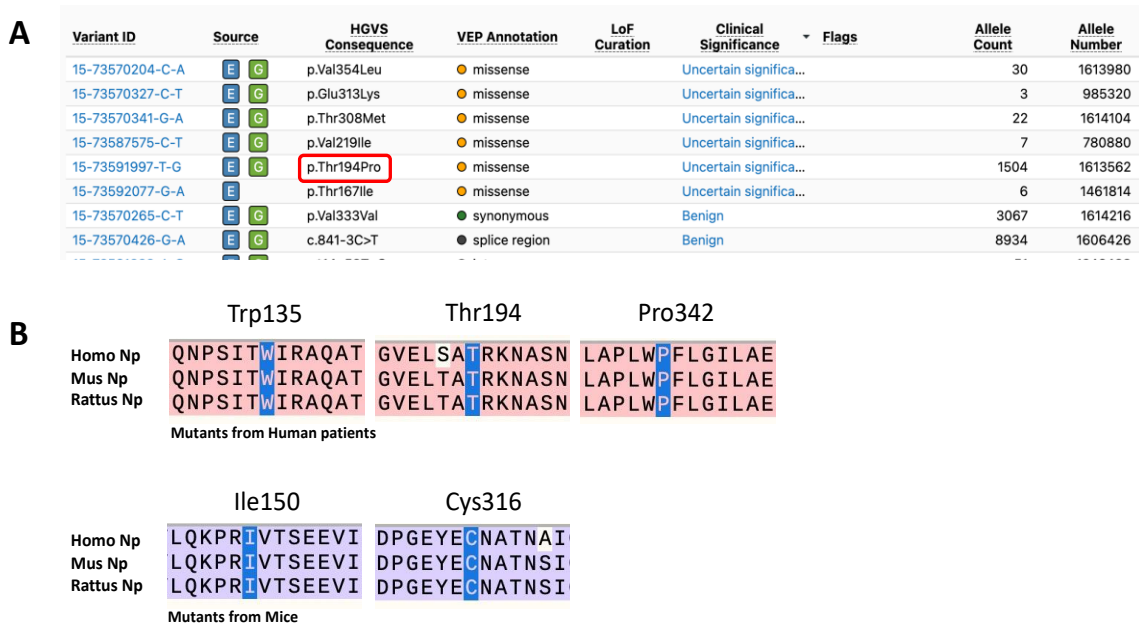


Figure 7: Reported mutations from database and alignment of Np sequences across different species

A. Summary of currently reported missense mutations in the database Clinvar and the analysis of the pathogenicity (Figure modified from <https://www.ncbi.nlm.nih.gov/clinvar/>). **B.** Analysis of the amino acid sequence homology for human, mouse, and rat Np surrounding the mutation sites. Localization of the amino acid alterations in the variants examined in this study are highlighted in blue. Variants from NDDs patients with the pink background. Variants from deaf mice with a purple background.

This series of experiments initiated from mutations causing hearing loss in mice. According to previous studies (Lin et al. 2021a; Newton et al. 2022; Zeng et al. 2016), Np55 is expressed in both IHCs and OHCs of the cochlea, Np65 is also expressed in the cochlea but the exact cellular location has not yet been clarified. Therefore, for the mutations associated with hearing damage, plasmids for expression of both isoforms hNp55 and hNp65 were constructed. Furthermore, plasmids of variants detected in human NDDs patients were also constructed (Fig.8).

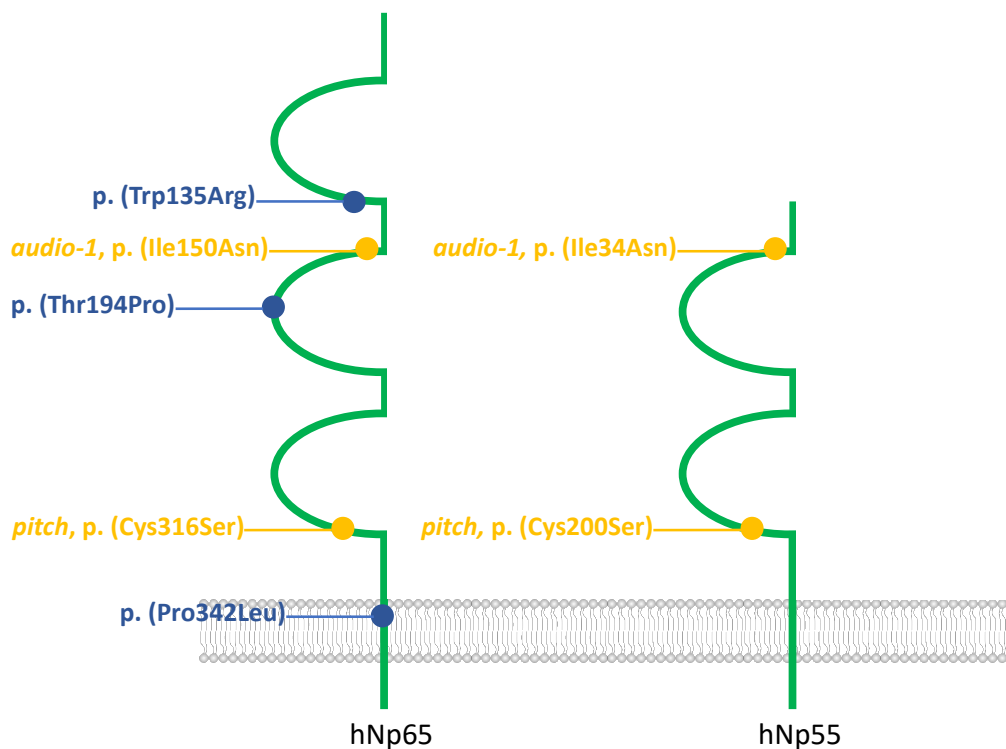


Figure 8: Schematic illustration of the variant's sites in two hNp isoforms

Here hNp55 and hNp65 displaying two and three Ig-domains, a single transmembrane and the cytoplasmic domain. Mutants from mice with hearing loss *pitch* and *audio-1* indicated in yellow. Variants from human NDDs patients p.W135R, p.T194P and p.P342L are labeled in blue. Five variants located in 1st, 2nd and 3rd Ig domain, respectively.

4.2. Reduced expression of mutated human Np and PMCA in HEK293T cells

To evaluate the variants' functionality and verify their potential harmful impact, experiments were performed using the human derived HEK293T cell line. By Western

blot analysis, the expression of hNp after transfection of HEK293T cells was revealed. Meanwhile, based on previous work (Herrera-Molina et al. 2017; Schmidt et al. 2017; Gong et al. 2018), it was shown that the protein levels of the four PMCA paralogs (PMCA1-4) strongly depend on binding to Np and the formation of stable protein complexes with Np. As expected, both hNp55^{WT} and hNp65^{WT} promoted the PMCA2-GFP levels in co-transfected HEK293T cells (Fig.9 A, D), which was consistent with the results obtained from a previous study (Herrera-Molina et al. 2017). Besides, it was also examined here whether exogenous PMCA2-GFP levels can be promoted by hNp55/65^{pitch} or hNp55/65^{audio-1}. Interestingly, for Np expression level, both hNp55^{pitch} and hNp65^{pitch} were expressed at levels similar to hNp55/65^{WT}, but the expression of PMCA2-GFP was significantly decreased in hNp55/65^{pitch} co-transfected HEK293T cells (Fig.9 B, C, E, F).

The expression of Np in the mutated hNp55/65^{audio-1} showed a significant reduction compared to the hNp55/65^{WT}. Meanwhile, the expression level of PMCA2-GFP was also decreased in hNp55/65^{audio-1} compared with hNp55/65^{WT} (Fig.9 B, C, E, F). In addition, the band of hNp55^{audio-1} was almost undetectable after short exposure time, and only revealed when the exposure time was extended to >30s (Fig.9 A).

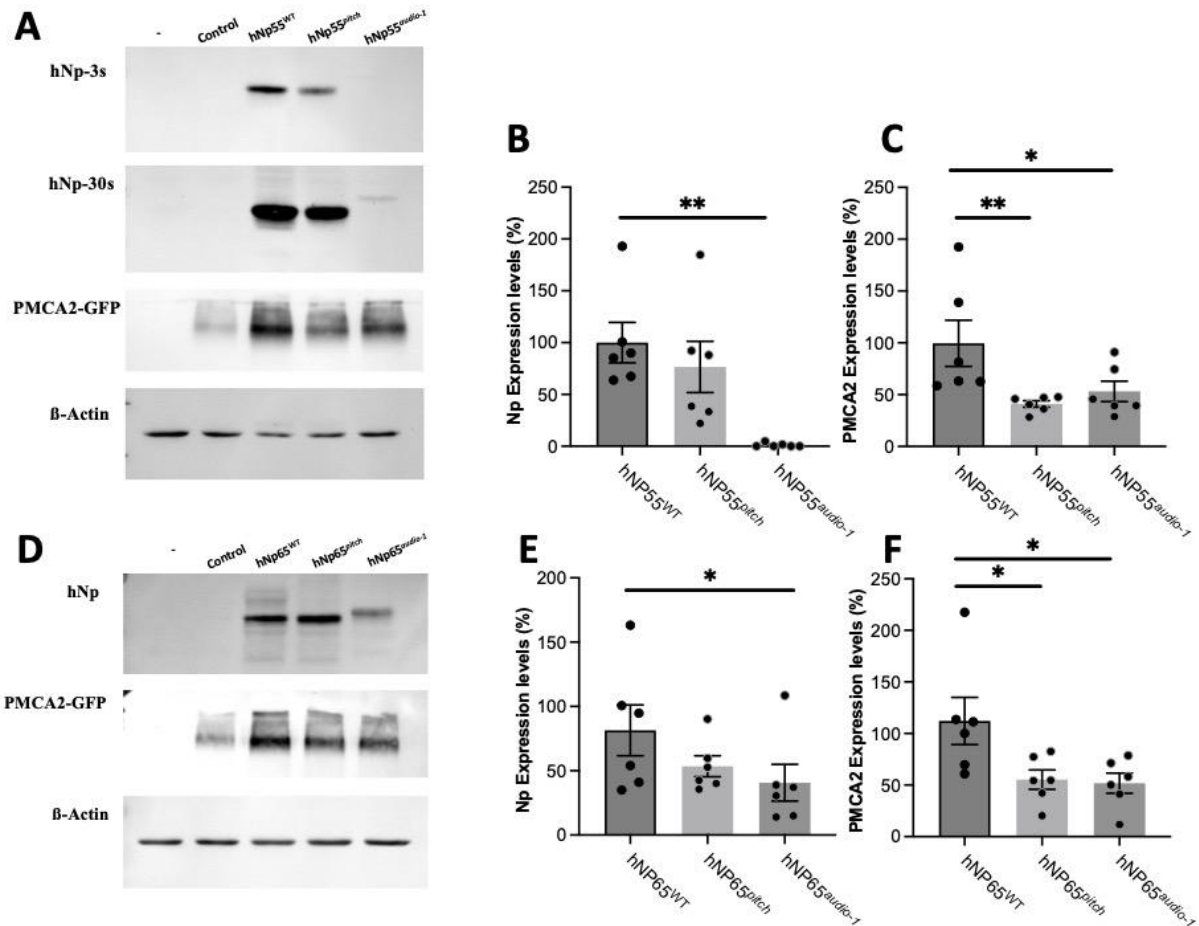


Figure 9: Western blot analysis of Np and PMCA in HEK293T cells transfected with PMCA2-GFP or co-transfected with PMCA2-GFP and hNp variants from hNp55/65^{pitch} and hNp55/65^{audio-1}

A. Western blots for the hNp55 isoform, β -actin staining served as a loading control. Np is shown after expose of 3s and 30s. **B, C.** Quantification of Np and PMCA-GFP protein expression levels by densitometric analysis of Western blots from six independent transfection experiments, which displayed significantly less expression of Np in hNp55^{audio-1} and the less capacity in both hNp55^{pitch} and hNp55^{audio-1} to promote PMCA2-GFP levels compared with hNp55^{WT}. **D.** Western blots for the hNp65 isoform, β -actin staining served as a loading control. **E, F.** Quantification of Np and PMCA-GFP protein expression levels by densitometric analysis of Western blots from six independent transfection experiments, which displayed significantly less expression of Np in hNp55/65^{audio-1} and the less capacity in both hNp65^{pitch} and hNp65^{audio-1} to promote PMCA2-GFP levels compared with hNp65^{WT}. Data are represented as mean \pm SEM with * indicates $p < 0.05$, ** indicates $p < 0.01$.

The NDDs human patients' variants were investigated under the same conditions in HEK293T cells transfected with PMCA2-GFP or co-transfected with PMCA2-GFP. The results showed that the expression levels of Np and PMCA2-GFP for both hNp^{p.W135R} and hNp^{p.P342L} were significantly reduced compared to hNp65^{WT}, while variant hNp^{p.T194P} expressed similar levels as hNp65^{WT} (Fig.10).

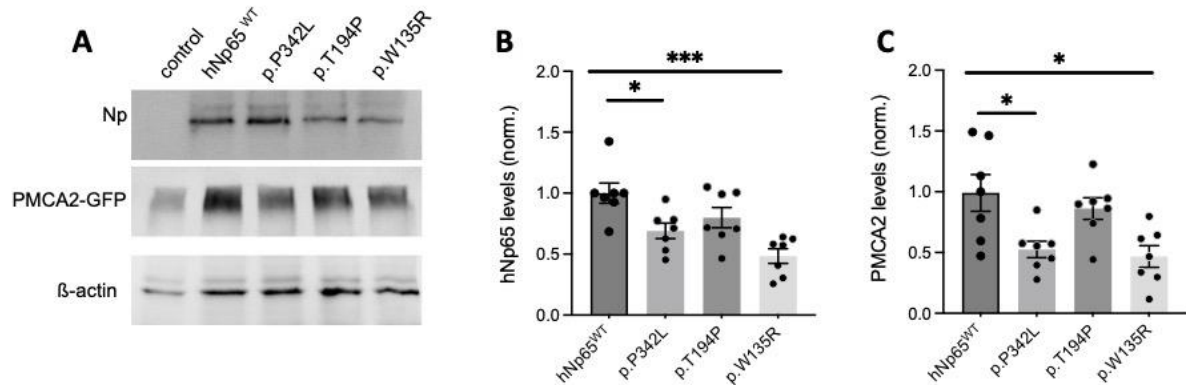


Figure 10: Western blot analysis of Np and PMCA in HEK293T cells transfected with PMCA2-GFP or co-transfected with PMCA2-GFP and hNp variants from human patients

A. Western blot of homogenates from HEK293T cells, β -actin staining served as a loading control. **B,C.** Quantification of Np and PMCA protein expression levels by densitometric analysis of Western blots from seven independent transfection experiments, which displayed significantly less expression of hNp^{p.W135R} and hNp65^{p.P342L}, also with lower capacity of hNp^{p.W135R} and hNp65^{p.P342L} to promote PMCA2-GFP levels compared with hNp65^{WT}. Data are represented as mean \pm SEM with * indicates $p < 0.05$, *** indicates $p < 0.001$.

4.3. Altered glycosylation of hNp55/65^{audio-1}

According to Western blots, an aberrant migration of the bands corresponding to hNp55/65^{audio-1} was always observed corresponding to a higher molecular weight of hNp55/65^{audio-1} (Fig.9A, D, Fig11). The change of isoleucine to asparagine in the *audio-1* variant possibly resulting in additional glycosylation (from to “Ile-Val-Thr” to “Asn-Val-Thr”). To confirm this assumption, treatment with PNGase F, one of the most effective enzymatic methods for removing almost all N-linked oligosaccharides from glycoproteins, was applied. After enzymatic digestion, the bands corresponding to both isoforms hNp55^{audio-1} and hNp65^{audio-1} migrated at the same level as hNp55/65^{WT} (Fig.11).

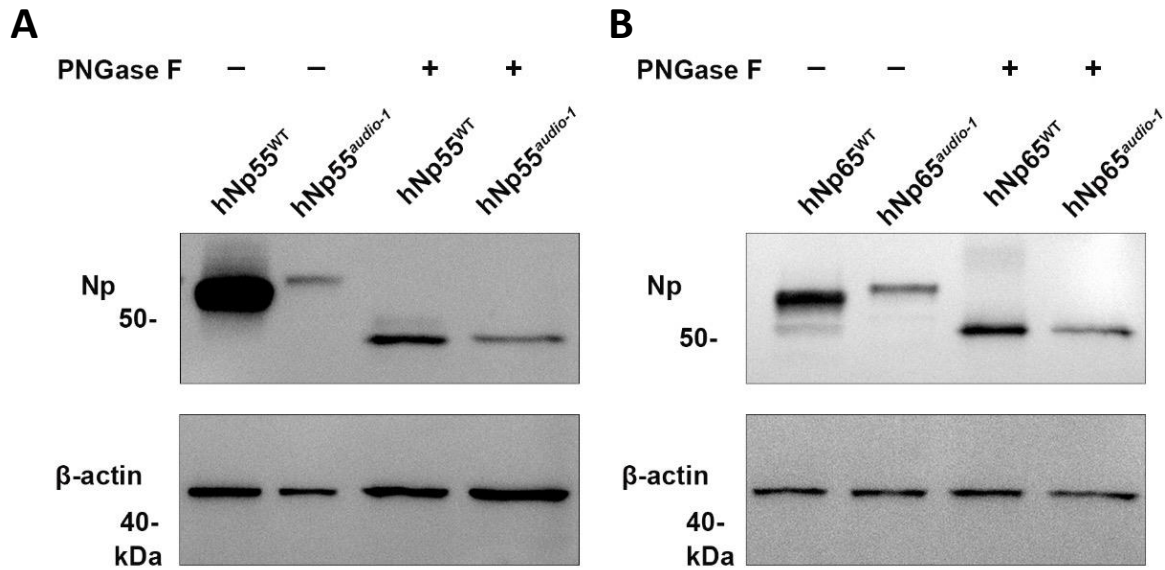
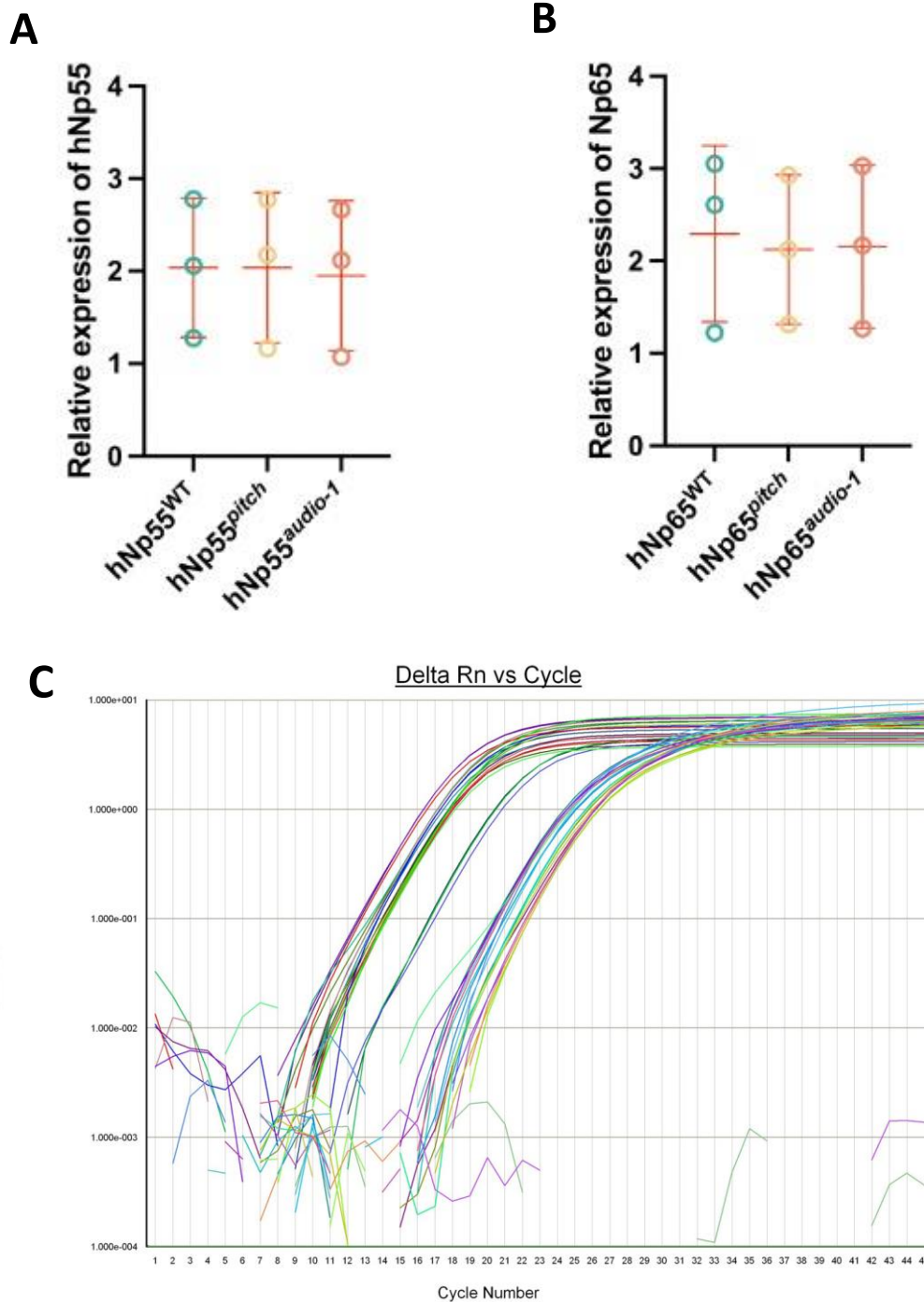


Figure 11: Western blot of PNGaseF treatment from HEK293T cells

A. the hNp55 isoform, **B.** the hNp65 isoform. Before the PNGaseF treatment, hNp55/65^{audio-1} showed a noticeably heavier molecular weight as hNp55/65^{WT}. After deglycosylation by N-glycosidase PNGaseF treatment, *audio-1* variants migrated at the same molecular weight as their corresponding hNp55/hNp65^{WT}, β -actin staining served as a loading control.

4.4. Causes of reduced Np expression

The decreased expression of the mutated hNp may be explained by two hypotheses. First, a decrease in transcription may lead to less mRNA and protein synthesis or second, enhanced degradation of unstable or aberrant proteins may occur. To explore the impact of hNp variants on RNA transcription, splicing, and stability, real-time PCR was conducted using total RNA extracted from transfected HEK293T cells. The primers employed in this study were positioned within exons 4 and 5. The level of Np mRNA was not significantly different between hNp^{WT} and the hNp variants for both hNp55/65^{pitch} and hNp55/65^{audio-1} (Fig.12).



Selected Detector: All
 Document: 2023.10.31 Plate2 study (ddCt Study)

Figure 12: RT-PCR analysis of hNp55/65^{WT}, hNp55/65^{pitch}, hNp55/65^{audio-1}

A. Quantification of Np mRNA from three independent hNp55 plasmid transfection experiments. **B.** Quantification of Np mRNA from three independent hNp65 plasmid transfection experiments. **C.** The raw amplification plot of all samples from the RT PCR7300 system software. The plot contains the amplification curves including all detectors, standard references and negative controls from hNp55/65^{WT}, hNp55/65^{pitch} and hNp55/65^{audio-1} in 3 duplicates. The cycle numbers for reactions were 45 cycles.

Combining protein structure modelling and molecular dynamics simulation (in collaboration performed by Dr. Ormazábal-Toledo R; data not shown), another reason for the reduction in protein expression amounts indicated that the mutation caused amino acid changes reduce the structural stability of the proteins, ultimately resulting in more degradation. Therefore, treatment with protease inhibitors (MG132) and lysosomal inhibitor (NH₄Cl) was used to assess whether blocking the hydrolysis of the proteins would normalize the amount of hNp protein. After the inhibitor treatment, increased levels of hNp55^{WT}, hNp55^{pitch}, and hNp55^{audio-1} were detected (Fig.13), indicating Np could be hydrolyzed *via* both proteasome and lysosomal pathways. Furthermore, in hNp55^{WT}, variants hNp55^{pitch}, and hNp55^{audio-1}, cells treated with MG132 expressed more Np than those treated with NH₄Cl, which may reveal that the proteasome pathway is the more dominant pathway for Np protein degradation (Fig.13).

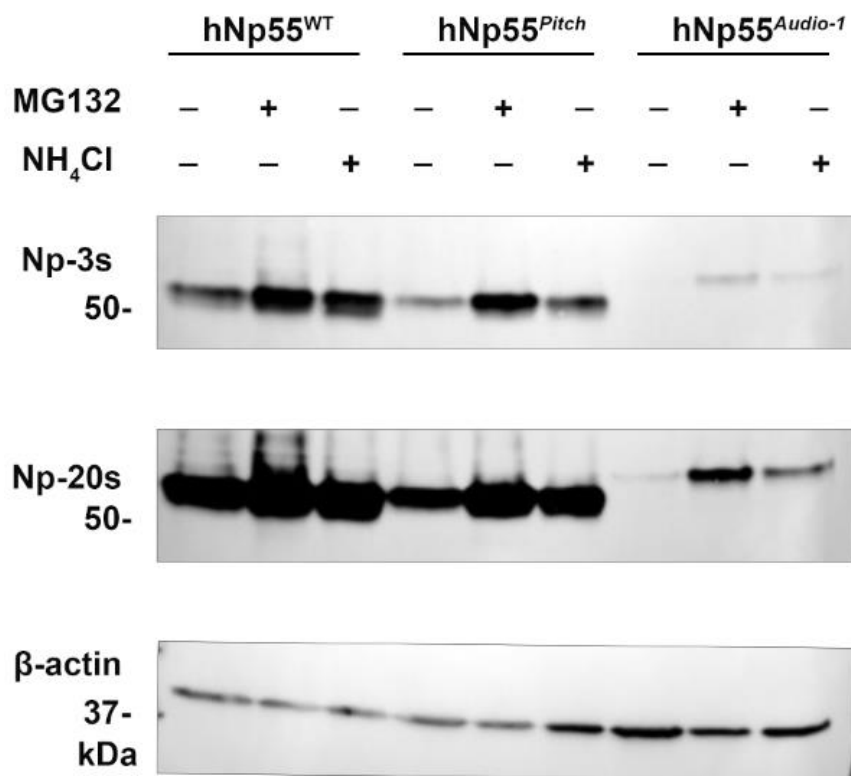


Figure 13: Western blot of Proteasomal (MG132) or lysosomal (NH₄Cl) inhibitor treatment from HEK293T cells

HEK293T cells were transfected with hNp55^{WT}, hNp55^{pitch} or hNp55^{audio-1}. After 6 hours-treatment with the inhibitor, the levels of hNp55^{WT}, hNp55^{pitch}, and hNp55^{audio-1} all increased compared to negative control. Np blots exposure time was 3s, and for signal saturation 20s. β -actin staining served as a loading control.

4.5. Overexpression of mutated Np reduced the expression of hNp and PMCA in neurons and failed to promote endogenous PMCA levels leading to altered basal cytosolic Ca²⁺-level restoration in neurons

To investigate the impact of specific variants on cytosolic Ca²⁺ signaling, calcium imaging studies in hippocampal neuron cultures were conducted. Hippocampal primary neurons were co-transfected at DIV11 with plasmids encoding either the hNp65^{WT} or one of the variants and RFPT-P2A-GCaMP5, serving as a calcium indicator. 3-4 days after transfection, the neurons were depolarized to trigger an influx of Ca²⁺, leading to the subsequent appearance of cytosolic Ca²⁺ transients, registered following protocols and methods established by Malci et al., 2022. These transient events are ultimately reflecting the activity of PMCA (Herrera-Molina et al. 2017; Schmidt et al. 2017). Ca²⁺ transients were firstly triggered with a low frequency electrical stimulation (LFS, 10 Hz) for the two mutants *pitch* and *audio-1* compared to hNp^{WT}. The Ca²⁺ transients of the dendrites were analyzed using the software ImageJ and Clampfit (Fig.14).

The results showed that the decay time, half width, and peak amplitude of the Ca²⁺ transients were significantly reduced in hNp65^{WT} transfected neurons compared to control neurons (Fig.15 A-C), which is consistent of Np-promoted PMCA-mediated Ca²⁺ clearance as described before (Herrera-Molina et al. 2017; Schmidt et al. 2017; Malci et al. 2022). In contrast, hNp65^{*pitch*} transfected neurons displayed an extended decay time, half width, and higher peak amplitude compared to hNp65^{WT} transfected neurons (Fig.15 A-C). While hNp65^{*audio-1*} transfected neurons displayed a similar accelerated Ca²⁺ extrusion and comparable decay time with hNp65^{WT} transfected neurons (Fig.15A), which may indicate sufficiently increased PMCA activity in hNp65^{*audio-1*} transfected neurons.

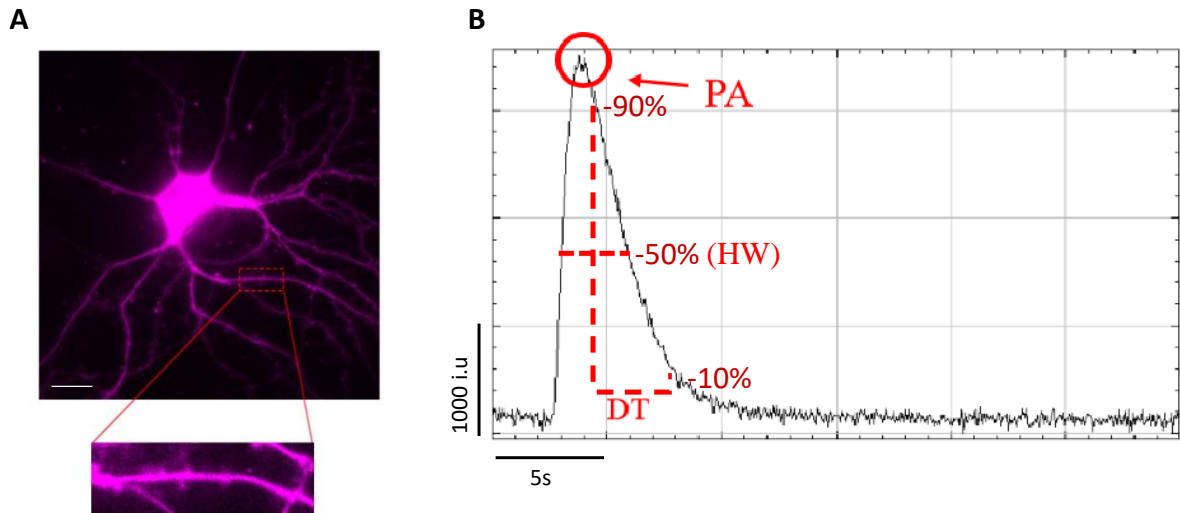


Figure 14: An example of calcium imaging of a hippocampal neuron and schematic diagram of calcium kinetic analysis

A. An example of observing the GCaMP channel for a hippocampal neuron at DIV 14 which had been transfected with RFPT-GCaMP5 and hNp65^{WT} at DIV11. The observation occurred after stimulation, during which the transient decay activity was recorded. Scale bar=10 μm . **B.** The process utilized Axon™ pCLAMP™ 10.7.0 Electrophysiology Data Acquisition and Analysis Software (Molecular Devices) to quantify Ca^{2+} activity. Throughout the experiment, both the baseline and signal region for each observation were consistently defined using the cursors provided in the pCLAMP software. Key metrics Decay Time (DT; in ms), Half-Width (HW; in ms), and Peak Amplitude (PA) were measured for each observed dendrite. For the purpose of final data presentation, these values were normalized. The software provided "baseline cursors" to identify the average baseline. "Signal cursors" were positioned at the points of stimulation, and the software then determined the peak amplitude relative to this baseline. The half-width was automatically calculated by the software, using 50% of the peak amplitude for its measurement. The decay time was calculated between the "90%" and "10%" signals.

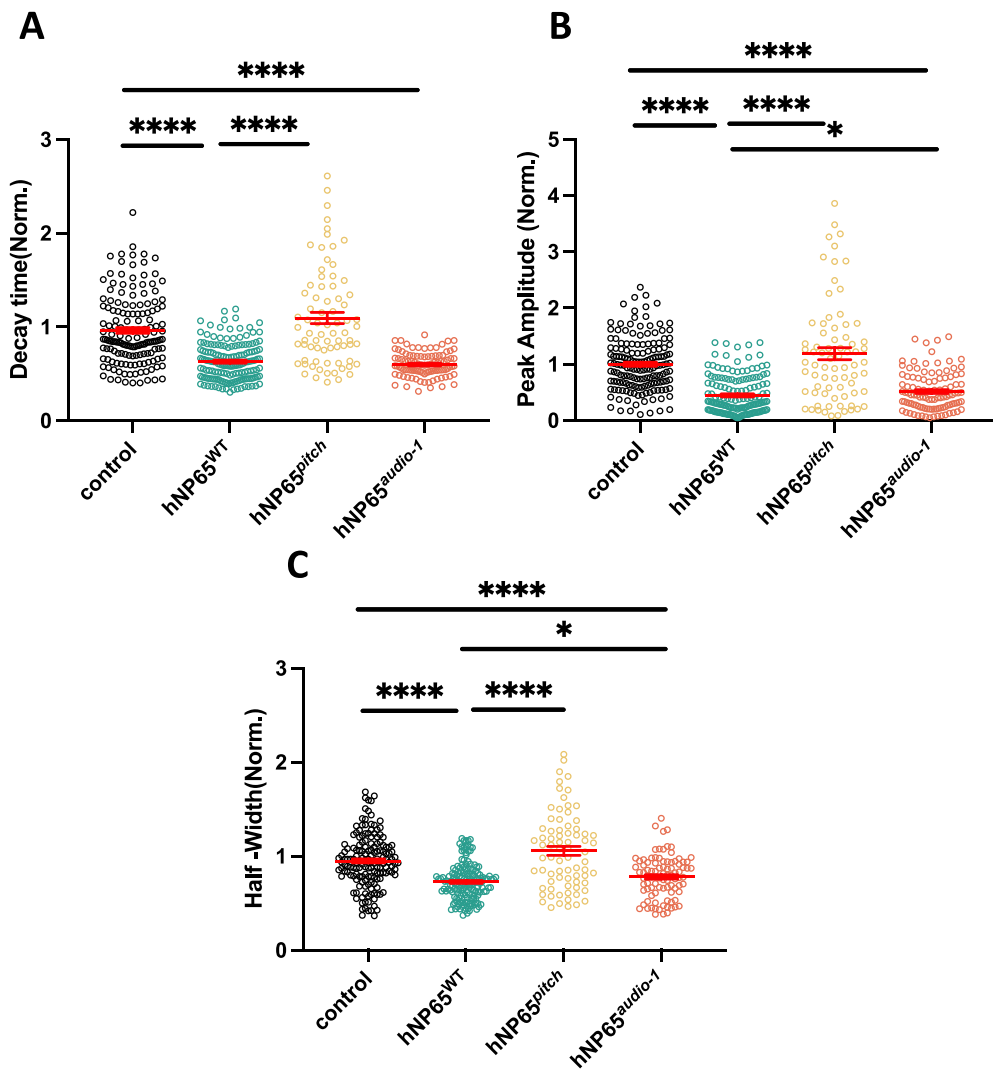


Figure 15: LFS condition calcium imaging analysis in hNp65^{pitch} and hNp65^{audio-1} transfected hippocampal neurons

A. Decay time **B.** Half width and **C.** Peak Amplitude of electrically-evoked cytosolic Ca²⁺ transient in dendrites in LFS condition. Data are represented as mean ± SEM with * indicates p<0.05, **** indicates p<0.0001.

To test further the efficiency of hNp65^{audio-1} for Ca²⁺ extrusion, higher frequencies of electrical stimulation (HFS, with 20/100 Hz) were applied (Fig.16). As expected, overexpression of hNp65^{WT} still reduced the decay time, half width, and peak amplitude of the Ca²⁺ transients compared with control group. Whereas after HFS, hNp65^{audio-1} transfected neurons were largely inefficient to extrude Ca²⁺ (Fig.16).

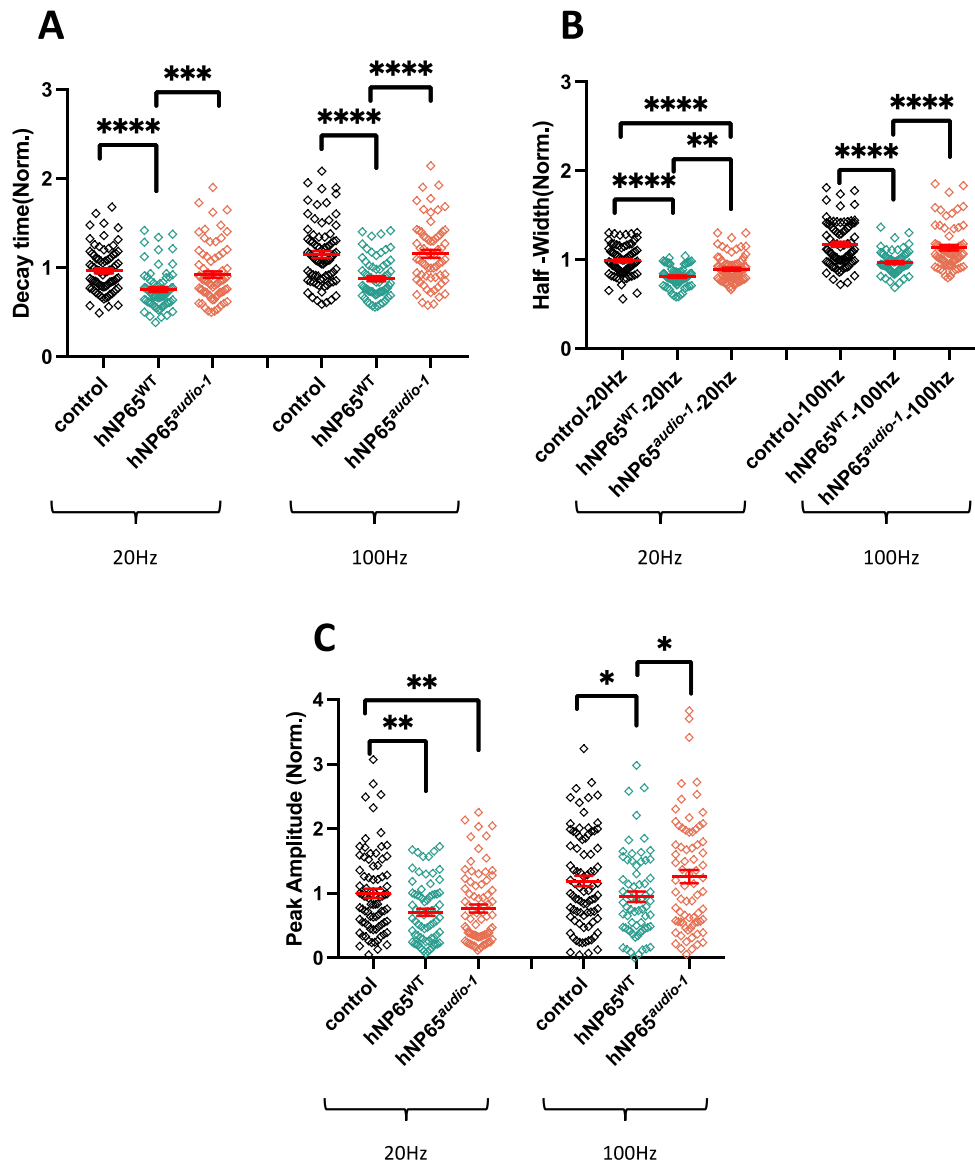


Figure 16: HFS condition calcium imaging analysis in variant hNp65^{audio-1} transfected hippocampal neurons

A. Decay time, **B.** Half width and **C.** Peak Amplitude of electrically-evoked cytosolic Ca²⁺ transient in dendrites in HFS condition. Results are shown after 20Hz and 100Hz stimulation. Data are represented as mean ± SEM with * indicates p<0.05, ** indicates p<0.01, *** indicates p<0.001, **** indicates p<0.0001.

Furthermore, co-transfection with a GFP-expressing plasmid served to identify transfected neurons. Immunohistochemical analysis revealed that the transfection with hNp65^{pitch} and hNp65^{audio-1} led to a reduced expression of Np compared to cells transfected with hNp65^{WT} (Fig.17).

Based on the above experiments, considering the possibility that the LFS condition may be not sufficient to expose the effect of the variants on Ca²⁺ efflux, the variants from the human patients were also analyzed in the HFS condition. The variant hNp65^{p.W135R} displayed a significant increase in the decay time, peak amplitude and half width. While variants hNp65^{p.P342L} and hNp65^{p.T194P} showed an accelerated Ca²⁺ extrusion comparable to hNp65^{WT} neurons even in the HFS condition (Fig.18).

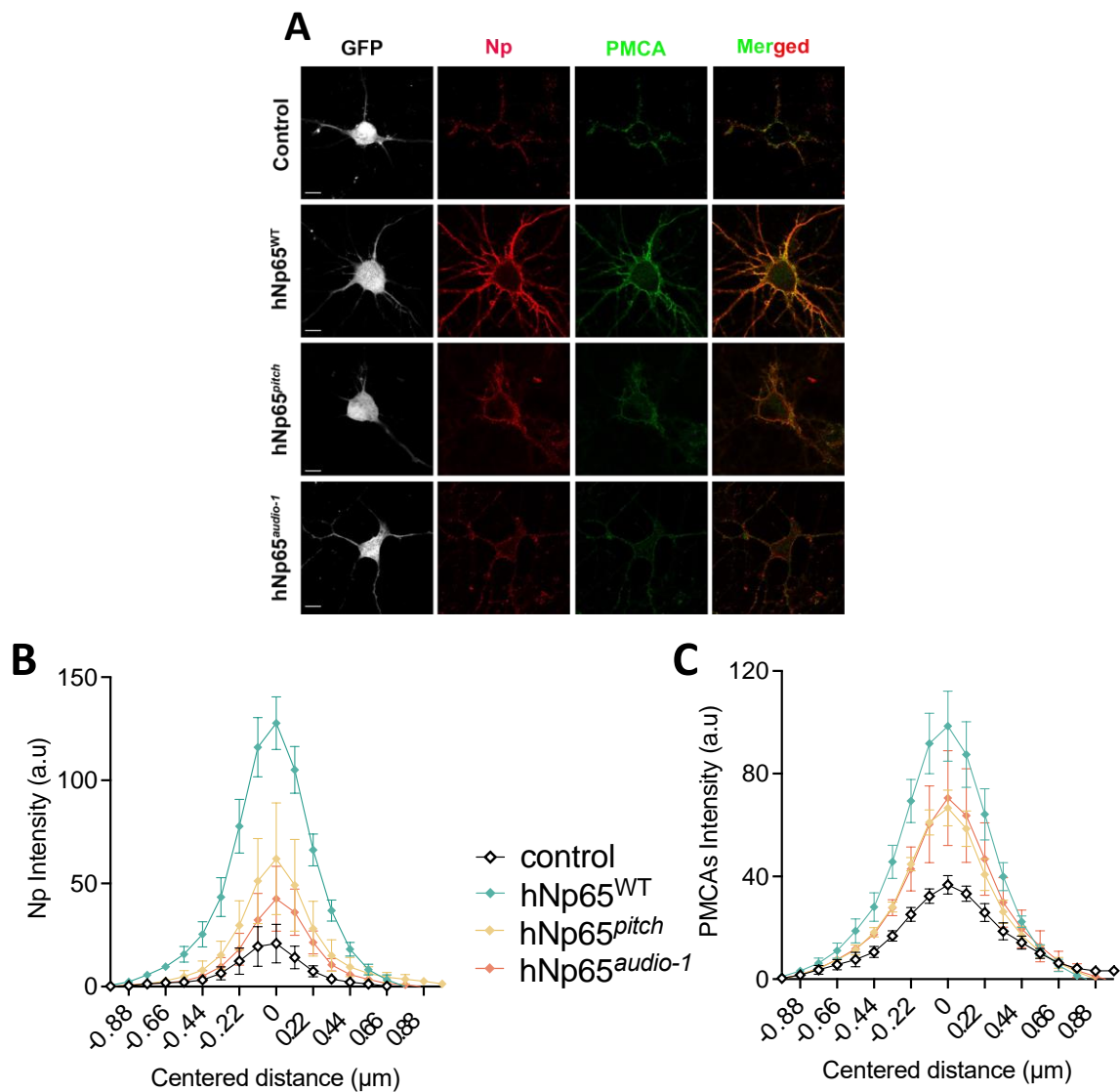


Figure 17: Immunohistochemical staining and quantification of Np and PMCA intensity in hippocampal neurons

A. Confocal microscopy pictures of primary hippocampal neurons transfected with GFP or co-transfected with either hNp65^{WT}, hNp65^{pitch} or hNp65^{audio-1}, fixed and immunostained for hNp (red) and PMCA (green) at DIV14. hNp65^{WT} promoted Np and PMCA immunoreactivities but hNp65^{pitch} and hNp65^{audio-1} showed less promotion. Scale bar=10 μm. **B,C.** Quantification of immunohistochemical results for Np and PMCA expression from three independent transfection experiments (Np intensity: control vs. hNp65^{WT} $p < 0.0001$; control vs. hNp65^{pitch}, $p < 0.05$; control vs. hNp65^{audio-1}, $p < 0.05$; hNp65^{WT} vs. hNp65^{pitch}, $p < 0.0001$; hNp65^{WT} vs. hNp65^{audio-1}, $p < 0.0001$; PMCA intensity: control vs. hNp65^{WT} $p < 0.001$, control vs. hNp65^{pitch}, $p < 0.0001$; control vs. hNp65^{audio-1}, $p < 0.01$; hNp65^{WT} vs. hNp65^{pitch}, $p < 0.001$, hNp65^{WT} vs. hNp65^{audio-1}, $p < 0.001$).

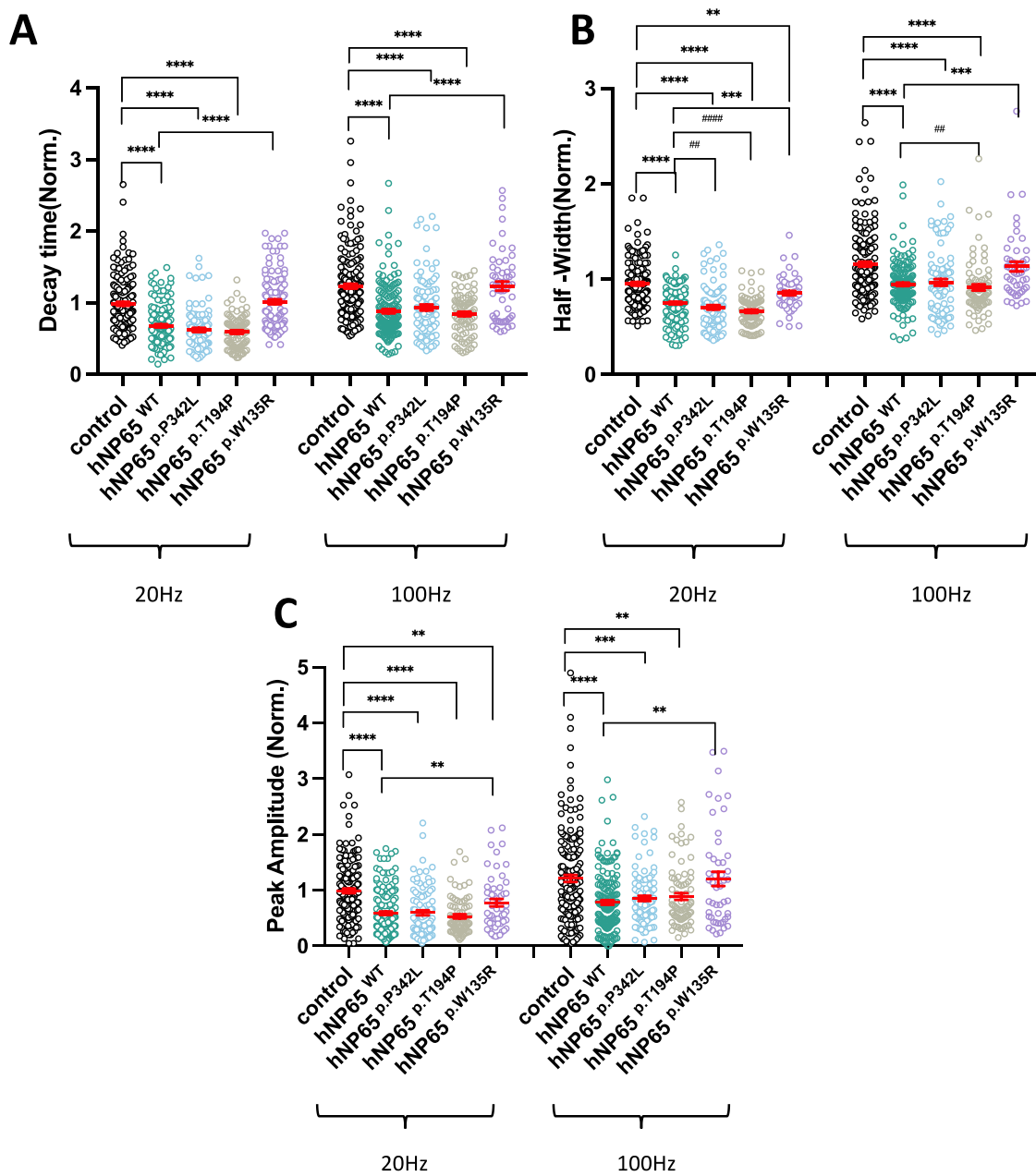


Figure 18: HFS condition calcium imaging analysis in variants hNp65^{p.W135R}, hNp65^{p.P342L} and hNp65^{p.T194P} transfected hippocampal neurons

A. Decay time, **B.** Half width and **C.** Peak Amplitude of electrically-evoked cytosolic Ca²⁺ transient in dendrites in HFS condition. Results are shown after 20Hz and 100Hz stimulation results. Data are represented as mean ± SEM with * indicates p<0.05, ** indicates p<0.01, *** indicates p<0.001, **** indicates p<0.0001.

4.6. Np-siRNA knock-down experiments for human variants

Since Np65 is specifically expressed in the neurons of brain, another explanation for the comparable changes in the promotion of Ca^{2+} efflux by both hNp65^{p.P342L} and hNp65^{p.T194P} variants compared to hNp65^{WT} may be that the amount of endogenous Np in neurons is already sufficient for the efflux of intracellular calcium ions. Thus, exogenous overexpression of Np may not really reflect and indicate a potential alteration.

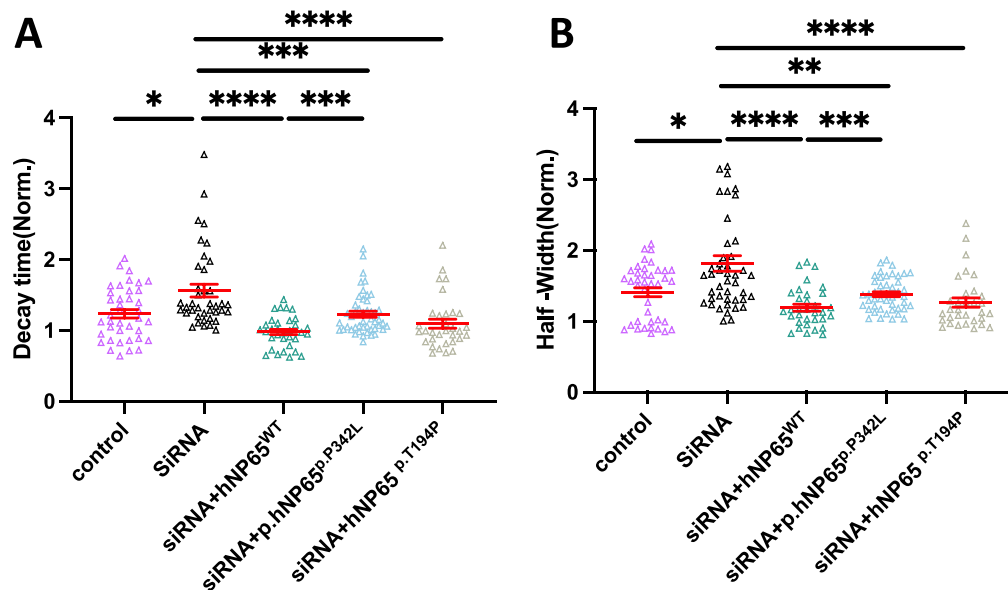


Figure 19: 100Hz HFS condition calcium imaging analysis in Np-siRNA and variants hNp65^{p.P342L} or hNp65^{p.T194P} transfected hippocampal neurons

A. Decay time, **B.** Half width of electrically-evoked cytosolic Ca^{2+} transient in dendrites in 100Hz HFS condition. Data are represented as mean \pm SEM with * indicates $p < 0.05$, ** indicates $p < 0.01$, *** indicates $p < 0.001$, **** indicates $p < 0.0001$.

To evaluate this, rat hippocampal neurons were co-transfected with the plasmids PGP-CMV-jGCaMP7, Np-siRNA and hNp constructs on DIV10. On DIV14, calcium imaging was done to record the calcium clearance. The neurons were depolarized with 100 Hz. Interestingly, after Np-siRNA transfection neurons showed apparently increasing decay time and halfwidth compared to the control group, reflecting the role played by Np-siRNA in this condition reducing the endogenous Np expression. By co-transfection with exogenous hNp65^{WT}, the Ca^{2+} efflux capacity was restored compared to the siRNA knock down group. The exogenous variant hNp65^{p.P342L} exhibited some rescuing effects compared to the knock down group, but still showed increased decay

time and half width compared to the exogenous hNp65^{WT}. Moreover, exogenous variant hNp65^{p.T194P} still performed comparable as the exogenous hNp65^{WT} (Fig.19).

4.7. NPTN p.P>L variant displayed functional deficits in *Drosophila*

Interestingly, among all the variants mentioned above, p.P342L (Np65) is the only one mutated in the transmembrane region, which is one of the key sites for Np binding to PMCA. At the same time, the above experiments were all based on *in vitro* conditions, which differ from the actual *in vivo* environment. To analyze the effects of this mutation in an *in vivo* situation, constructs were generated for expression of this variant in *Drosophila* larval muscles. A hNp55^{WT} construct was generated to serve as a control. Both constructs were inserted into the same chromosomal position to ensure comparable rates of transcription.

In vivo expression of a bsg-specific RNAi construct in larval muscles was previously shown to cause muscle deficits similar to those observed, when PMCA is knocked-down (Bai et al. 2008; Schnorrer et al. 2010). These animals also display a severe reduction of PMCA in the postsynaptic compartment of the NMJs (personal communication with Dr. U. Thomas). Therefore, it was investigated here, whether transgenic expression of the hNp55^{WT} or hNp55^{p.P>L} could rescue the PMCA expression. Analysis of immunofluorescence staining of PMCA intensity at NMJs from third-stage larvae, confirmed that in the *bsg* knock down control group (C57-Gal4/UAS-*bsg*-RNAi), PMCA expression in NMJs is reduced by about 80% compared with the w1118 control group. However, the hNp55^{WT} rescue group (UAS-hNp55/+; UAS-*bsg*-RNAi/C57-Gal4) showed a perfect restoration of the PMCA expression level. In contrast, the hNp55^{p.P>L} rescue group (UAS-hNp55^{p.P>L} /+; UAS-*bsg*-RNAi/C57-Gal4) was clearly less efficient, showing only a statically non-significant increase in PMCA at NMJs (Fig.20).

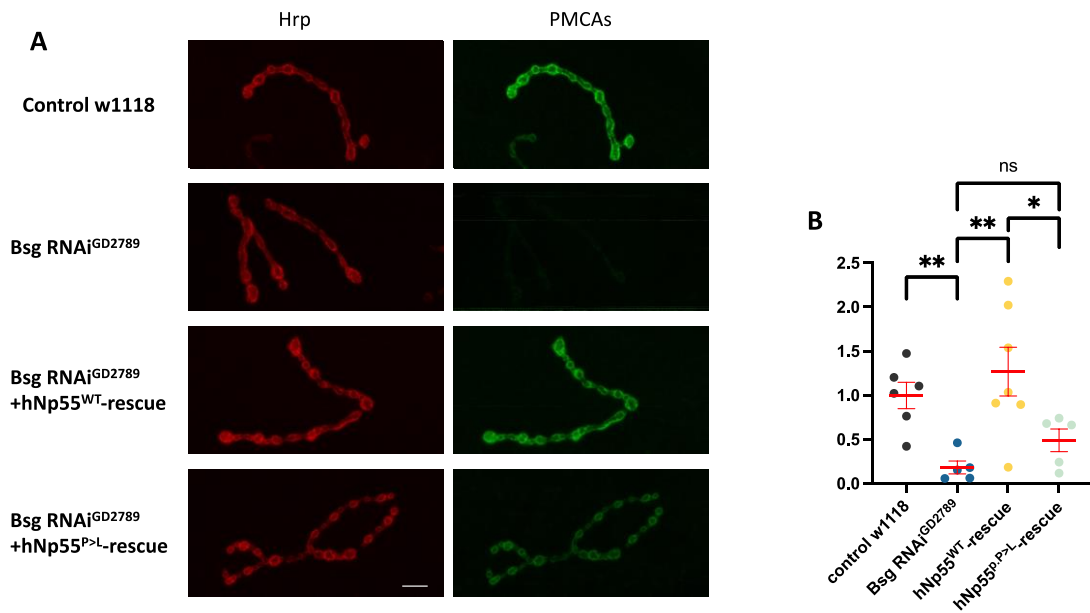


Figure 20: Immunohistochemical staining examples and quantification of PMCA intensity in *Drosophila* NMJs

A. Four sets of confocal pictures of NMJs stained for Hrp (red) and PMCA (green). Hrp staining served for the normalization of intensities. Scale bar=10 μ m. **B.** quantification of PMCA intensity in *Drosophila* NMJs: control w1118 (n=6 animals), Bsg RNAi^{GD2789} (n=5 animals), Bsg RNAi^{GD2789}+hNp55^{WT}-rescue (n=7 animals), Bsg RNAi^{GD2789}+hNp55^{P>L}-rescue (n=5 animals). Quantification of PMCA protein expression levels by densitometric analysis. mean \pm SEM. values; * indicates $p < 0.05$, ** indicates $p < 0.01$.

5. Discussion

Previously, it has not been reported that missense mutations in human *NPTN* cause any neurological disease. The research presented here originated as a study of the molecular mechanisms underlying the hearing deficits caused by *Nptn* mutations in mice. And further explored the effects of an abnormal binding relationship between Np and PMCA leading to impaired Ca^{2+} homeostasis in human potential hearing and neurological disorders. Combined with clinical data from collaborating physicians and molecular dynamics structure simulations researcher, the underlying molecular pathogenesis of human *NPTN* gene variants from phenotype to genotype can now be well explained.

5.1. Reduced PMCA and mutant Np protein expression levels are due to accelerated degradation resulting from protein structural changes

According to the public database (Clinvar), there are several *NPTN* gene mutation sites and types. The ones investigated here are interestingly located in the first (p.W135R), second (*audio-1*, p.T194P), third (*pitch*) Ig domains and at the transmembrane region (p.P342L), which is representative to some extent.

First, the expression level of mutated hNp and PMCA2 for all variants were examined in transfected HEK293T cells. The amount of PMCA expression with hNp^{WT} transfection matched those observed in earlier studies reporting that the stability and expression levels of PMCA are markedly influenced by their ability to form stable protein complexes with Np (Herrera-Molina et al. 2017; Schmidt et al. 2017; Malci et al. 2022; Gong et al. 2018). At the same time, the Np expression level of the variants hNp55/65^{*audio-1*}, hNp65^{p.P342L} and hNp65^{p.W135R} was decreased compared to hNp65^{WT}. In addition, these variants also caused a significant decrease in the expression of PMCA compared to hNp^{WT} Which promoted PMCA expression. The initial hypothesis involved a potential Np reduction caused by the missense mutations during the transcription phase. However, for the two deafness causing mouse mutations hNp^{*pitch*} and hNp^{*audio-1*}, the Np mRNA levels showed no reduction compared to hNp^{WT} mRNA.

Intriguingly, the hNp55/65^{pitch} expression was not significantly different from that of hNp55/65^{WT}, although there was a slight trend to reduction. In contrast, the expression level of PMCA was reduced. Another contributing factor to diminished protein expression levels might be that the different amino acid introduced by the mutation may lead to decreased structural stability of the proteins, which consequently results in their increased degradation. According to the unpublished data from protein structure prediction and molecular dynamics simulation by collaborator Dr. Ormazábal-Toledo R, more details of the structural changes of the variants hNp proteins were described. For mutant hNp^{audio-1}, the steric hindrance caused by the amide group of N150 leads to a shift towards the outer surface of hNp^{audio-1} IgII and creates a new site accessible to potential N-glycosylation (change from to “Ile-Val-Thr” to “Asn-Val-Thr”). This alteration could potentially lead to even more pronounced conformational changes and the additional carbohydrates may shield the protein surface interfering with binding partners. Consistent with the prediction of additional N-glycosylation in *audio-1* variants, both hNp65^{audio-1} and hNp55^{audio-1} exhibited a higher molecular weight compared to their respective controls, hNp55/65^{WT} in transfected HEK293T cells. Furthermore, removal of N-linked carbohydrates by PNGaseF treatment proved that this difference in molecular mass was caused by glycosylation. In addition, expression of hNp55^{audio-1} was very little or even almost disappeared, with faint bands visible only at extended exposure times. This may be due to the site of the mutation in IgII, which is immediately preceded and potentially protected by Igl in isoform hNp65^{audio-1}. While in isoform hNp55^{audio-1}, this site is close to the N-terminus and could be more easily degraded.

The protein modeling of the hNp^{WT} IgII-III domains revealed the presence of seven β -sheet structures that culminate in the formation of β -barrels, a structural motif known for its stability in immunoglobulins. This stability is significantly enhanced by conserved disulfide bridges, which are crucial to maintain the integrity of the protein structure. However, the *pitch* mutation led to conversion of cysteine to serine at position 316 (C316S) undermining this structural stability. In hNp^{pitch}, the critical disulfide bridge cannot form due to the absence of the cysteine residue. Consequently, this single amino acid change results in a protein that is structurally less stable compared with hNp^{WT}. The lack of this disulfide bond in the mutated Np contributes to an increased

vulnerability to degradation processes, further emphasizing the role of precise amino acid composition in protein stability and function.

Additionally, the stability of Np from the two deafness causing mutants were investigated with proteasome or lysosome inhibitors treatment. The use of MG132 and NH₄Cl revealed that the protein levels of hNp55^{WT}, hNp55^{*pitch*}, and hNp55^{*audio-1*} increase when proteasomal or lysosomal degradation is blocked. This indicates that *pitch* and *audio-1* mutations enhance the possibility for degradation.

Tryptophan is a very conserved amino acid residue in Ig-domains and plays an important structural role in the β -barrel. Therefore, for the p.W135R variant, changing tryptophan to arginine, the aromatic, hydrophobic structure totally changed into a basic, charged hydrophilic structure likely to alter the protein's normal functions or interactions.

In the variant p.P342L, changes in protein structure originate from proline's unique cyclic structure, which limits flexibility and induces turns in the protein chain, that is replaced with leucine's hydrophobic, branched-chain structure. This change can increase flexibility and enhance hydrophobic interactions within the protein, potentially stabilizing it or altering its folding (Fig.21 B).

These findings revealed the importance of post-transcriptional regulation in controlling protein levels and highlighted the impact of structural changes on protein stability following amino acid alterations.

5.2. The reduction in PMCA expression is caused by the decreased binding capacity of Np and PMCA

The precise interaction between Np and PMCA is fundamental for the proper localization and function of PMCA (Schmidt et al. 2017; Gong et al. 2018). The transmembrane domain (TM) of Np directly interacts with PMCA and is sufficient for the stability and membrane targeting of PMCA. The Np-TM and the tenth transmembrane segment (TM10) of human PMCA1 engage closely through several hydrophobic residues near the membrane's extracellular surface (Gong et al. 2018). P342 is the potential key site for the interaction between Np and PMCA (Fig.21).

Replacing a proline by a leucine could increase the flexibility of this region of the protein because leucine does not impose the same rigid constraints on the backbone that proline does. This increased flexibility could affect the protein's overall structure, especially if the proline was critical in maintaining a turn or a loop and further lead to the alteration of the binding site between Np and PMCA (Fig.21 A). In addition, the decrease of PMCA expression associated with this variant was stronger than the decrease in hNp expression. Thus, in addition to the above-mentioned increased degradation of the p.P342L variant, the lower PMCA expression associated with p.P342L could also more likely originate from reduced stability of the Np-PMCA complex.

In addition, Np and PMCA as membrane proteins, interact with both the hydrophobic lipid bilayer of the cell membrane and the hydrophilic aqueous environment. This places higher demands on both protein structure prediction and molecular dynamics simulations to be carried out under suitable environments and conditions which later studies may explore.

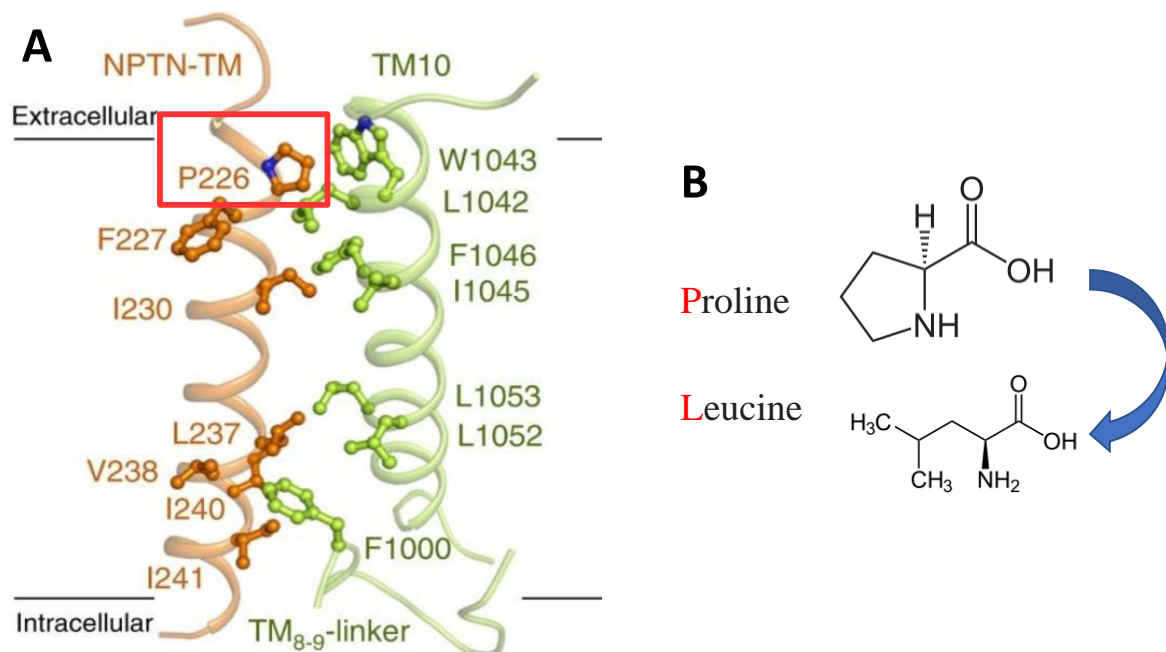


Figure 21: Schematic illustration of interactions between the transmembrane area of hPMCA1 and NPTN

A. NPTN-TM interacts with TM10 of PMCA, the hydrophobic residues on the interface are detailed. P226 could be the crucial binding site. Figure modified from (Gong et al. 2018).

B. amino acid changing from proline to leucine leads to the changing from the stabilized ring structure to a chain structure, and therefore reducing the stability.

5.3. *NPTN* mutations fail to promote endogenous PMCA levels and maintain basal cytosolic Ca²⁺ restoration in neurons

Recent evidence indicated that Np-PMCA complexes might be very critical for intracellular Ca²⁺ levels and in particular restoration of Ca²⁺ homeostasis after signaling (Herrera-Molina et al. 2017; Schmidt et al. 2017; Gong et al. 2018). Therefore, it was hypothesized that the effect of mutations in *NPTN* may lead to alterations in intracellular Ca²⁺ efflux mediated by PMCA that this underlies both deafness in the *Nptn* mouse mutants (Carrott et al. 2016; Zeng et al. 2016; Lin et al. 2021a) and the heterogeneous clinical phenotypes reported for patients with *NPTN* variants (personal communication with Dr. K. Platzer).

First, in the overexpression condition experiments, the introduction of hNp65^{WT} and the hNp65 variants into neurons aimed to assess how increased levels of these proteins affect Ca²⁺ extrusion mechanisms. Overexpression of hNp65^{WT} was found to enhance the efficiency of Ca²⁺ extrusion consistent with previous work (Malci et al. 2022). In contrast, the structural destabilization of *pitch* variant Np due to the absence of disulfide bonds in the protein further hindered the interaction with PMCA leading to less efficient Ca²⁺ clearance. On the other hand, the *audio-1* mutation does not appear to adversely affect Ca²⁺ extrusion in the LFS condition. This may indicate that mutant *audio-1* NP resulted in sufficient PMCA expression to extrude Ca²⁺ from neurons under LFS conditions. However, when challenged with HFS conditions, the mutant hNp^{*audio-1*} also displayed a weaker calcium ion clearance compared to hNp^{WT}.

Considering the above results, for the variants in human patients, HFS condition calcium imaging experiments were then conducted. The results showed that the p.W135R variant apparently exhibited a very weak Ca²⁺ removing capacity, while the variants p.P342L and p.T194P were not compromised.

Moreover, due to the presence of endogenous Np in neurons, the deficit may have been hidden by this. The feasibility of Np siRNA Knockdown was demonstrated in experiments by H. Srinivasan. (Personal communication) showing significantly reduced Ca²⁺ excretion of neurons after siRNA knock-down of endogenous Np. Therefore, transfection experiments with Np constructs after knock-down of endogenous Np by Np-siRNA were then conducted. The exclusion of this interfering

factor provided a clearer picture of the role of exogenous hNp for both WT or variants. Ultimately, variant hNp65^{p.P342L} resulted in less ability to excrete Ca²⁺ compared to hNp65^{WT}, while hNp^{p.T194P} still remained unaffected.

In summary, the experiments using Np-overexpression and LFS, Np-overexpression and HFS, and Np-siRNA knock-down and HFS conditions gradually revealed the different abilities of the various variants to promote restoration of intracellular calcium levels in neurons.

In addition, immunofluorescence staining of neurons expressing the two-mouse deafening mutants hNp^{pitch} or hNp^{audio-1} also showed compared to hNp^{WT} significant less endogenous PMCA expression at the cell membrane, supporting reduced stability of PMCA in complexes with mutant hNp. Considering the function of Np in effective trafficking, similar experiments with the other variants could be conducted in the future and the co-localization of Np and PMCA in neurons could be also evaluated later.

5.4. Expression in *Drosophila* NMJs model revealed the reduced Np and PMCA in p.P>L mutation under the *in vivo* system

The *Drosophila* NMJs serves as an effective, genetically accessible model, offering a glimpse into the *in vivo* expression of PMCAs. The results here indicated that compared to hNp55^{WT}, the hNp55^{p.P>L} mutation indeed showed strongly reduced capacity to restore PMCA levels in the postsynaptic compartment when endogenous Bsg was knocked-down. Moreover, both h55Np^{WT} and hNp55^{p.P>L} were clearly detectable at NMJs and within muscles by anti-Np antibody, whereas non-transgenic controls showed no specific staining. Preliminary analysis implied that the expression level of hNp55^{p.P>L} levels are lower at NMJs than hNp55^{WT} (data unshown). As both forms are expressed from the same chromosomal locus and differ in only one base, it seems likely that the mutated form is less stable or inefficiently targeted to NMJs. In fact, a difference in the distribution of the two variants was observed (data unshown), with the immunofluorescence associated with variant hNp55^{p.P>L} displayed punctate-like appearance in the muscles, much more than the h55Np^{WT}. Whether this observation relates to impaired trafficking to the plasma membrane remains to be addressed in further detail.

5.5. Potential pathogenesis of mutant Np in auditory deficits and NDDs

It is now well established that mutations in the *ATP2B/Atp2b* gene cause hearing abnormalities or neurological disorders in humans and rodents (Schultz et al. 2005; Smits et al. 2019; Rahimi et al. 2022; Poggio et al. 2023). There is also substantial evidence for altered levels of Np protein expression in a variety of neurodevelopmental or degenerative disorders (Desrivieres et al. 2015; Ilic et al. 2019; Ilic et al. 2021). This study has explored the molecular mechanisms PMCA function changed by Np, which may contribute to the failure of Ca^{2+} homeostasis in human NDDs or potential hearing problems.

Based on feedback from clinicians, the phenotype of *NPTN* variant patients is highly heterogeneous, including onset in early childhood with a global developmental delay, motor development delay, speech development delay, autism, seizures and further deficits (unpublished information). There are of course a number of molecular partners that bind to and interact with Np as mentioned before (Beesley et al. 2014; Lin et al. 2021b). Therefore, a pathogenesis mediated by disturbed interactions with these molecules is also quite possible. Here, due to the important role of Ca^{2+} regulation in many signaling events in the nervous system, this research focused on the functional study of PMCA.

Recently, in two studies in rat models of epilepsy, Li et al. demonstrated that Np may exert its antiepileptic effects by inhibiting the internalization of $\alpha 1$ -containing GABA_ARs through binding to GABRA1 (Li et al. 2023). Doğanyığıt et al. on the other side, demonstrated that this may be due to problems in the mechanisms regulating the interaction of Np and GluA1 and may lead to problems in synaptic plasticity (Doganyigit et al. 2024). It is worthwhile to note that during conducting Ca^{2+} imaging experiments, attempts to simulate a very simple artificial epileptic-like environment by using a Mg^{2+} free recording buffer were also done. It was observed that some of the signals recorded indicated that the neuron transfected with hNp variants did show abnormal excitatory activity compared to the neuron transfected with hNp^{WT} (data not shown). Therefore, further experiments and studies on the potential epileptogenicity due to Np mutations could also be conducted in the future.

In summary, this research proposed for the first time that NDDs caused by mutations in the *NPTN* gene are a clinically and genetically heterogeneous group of disorders. The underlying molecular pathologic mechanisms of NDDs caused by Np variants impairing the PMCA levels and Ca^{2+} transients were explained and also nominated new candidates for future discovery and functional studies. It enhanced our understanding of Np-related NDDs, and potentially leads to new ideas for early detection and further novel treatments.

6. Zusammenfassung

In den letzten Jahren wurden die genetischen Faktoren für neurologische Entwicklungsstörungen (NDDs) erforscht. Kürzlich wurden Mutationen im Neuroplastin (*Nptn*, *NPTN*) bei Mäusen mit Hördefiziten und bei menschlichen Patienten, die an einer NDD leiden, entdeckt. Neuroplastin (Np) gehört zur Superfamilie der Immunglobuline und seine Expression ist für die Aufrechterhaltung der Expression der Calziumpumpe Plasmamembran- Ca^{2+} -ATPase (PMCA) und ihrer ordnungsgemäßen intrazellulären Lokalisation erforderlich. Dies steht in engem Zusammenhang mit der Regulierung der intrazellulären Ca^{2+} -Homöostase. Bisher wurde die molekulare Pathogenese von NDDs, die durch *NPTN*-Genmutationen verursacht werden, noch nicht erforscht. In dieser Arbeit wurden durch die Herstellung von Expressionskonstrukten, die Transfektion von HEK293T-Zellen und primären Hippocampus-Neuronen, die Anwendung von *in-vitro*-Calcium-Imaging-Techniken und die Schaffung mutierter *Drosophila melanogaster*-Linien die Expressionsniveaus von Np und PMCA für jede Variante sowie die Dynamik der Ca^{2+} -Extrusion unter verschiedenen Bedingungen (Überexpression, niederfrequente Stimulation, hochfrequente Stimulation und Np siRNA-Knockdown-Bedingungen) ermittelt. Die Ergebnisse zeigten, dass die Missense-Mutationen *pitch* (C315S) und *audio-1* (I122N) in *Nptn*; p.W135R und p.P342L in *NPTN* die Struktur und Funktion des Np-Proteins und des PMCA-Neuroplastin-Komplexes beeinträchtigen, was zu einer gestörten zellulären Ca^{2+} -Homöostase führt. Dies könnte der molekulare pathologische Mechanismus sein, der die Hörstörungen bei Mäusen und die menschlichen NDDs verursacht. In dieser Studie wird ein molekularer Mechanismus vorgeschlagen, der dem pathologischen Prozess der Degeneration der äußeren Haarzellen zugrunde liegt, der bei *Nptn*-Mausmutanten zu Taubheit führt, sowie der neurologischen Entwicklungsstörung, die mit pathologischen *NPTN*-Varianten einhergeht. Diese Arbeit vertieft unser Verständnis einer neuartigen NDDs und könnte neue Erkenntnisse für die Früherkennung und weitere innovative Behandlungen liefern.

7. Bibliography

1. Amuti, S., Y. Tang, S. Wu, L. Liu, L. Huang, H. Zhang, H. Li, F. Jiang, G. Wang, X. Liu, and Q. Yuan. 2016. 'Neuroplastin 65 mediates cognitive functions via excitatory/inhibitory synapse imbalance and ERK signal pathway', *Neurobiol Learn Mem*, 127: 72-83.
2. Bai, J., R. Binari, J. Q. Ni, M. Vijayakanthan, H. S. Li, and N. Perrimon. 2008. 'RNA interference screening in Drosophila primary cells for genes involved in muscle assembly and maintenance', *Development (Cambridge, England)*, 135: 1439-49.
3. Balog, M., S. Blazetic, V. Ivic, I. Labak, B. Krajnik, R. Marin, A. Canerina-Amaro, D. P. de Pablo, A. Bardak, R. Gaspar, K. F. Szucs, S. G. Vari, and M. Heffer. 2022. 'Disarranged neuroplastin environment upon aging and chronic stress recovery in female Sprague Dawley rats', *Eur J Neurosci*, 55: 2474-90.
4. Bateman, J. R., A. M. Lee, and C. T. Wu. 2006. 'Site-specific transformation of Drosophila via phiC31 integrase-mediated cassette exchange', *Genetics*, 173: 769-77.
5. Beesley, P. W., R. Herrera-Molina, K. H. Smalla, and C. Seidenbecher. 2014. 'The Neuroplastin adhesion molecules: key regulators of neuronal plasticity and synaptic function', *J Neurochem*, 131: 268-83.
6. Berrocal, M., I. Corbacho, M. Vazquez-Hernandez, J. Avila, M. R. Sepulveda, and A. M. Mata. 2015. 'Inhibition of PMCA activity by tau as a function of aging and Alzheimer's neuropathology', *Biochimica Et Biophysica Acta*, 1852: 1465-76.
7. Besse, F., S. Mertel, R. J. Kittel, C. Wichmann, T. M. Rasse, S. J. Sigrist, and A. Ephrussi. 2007. 'The Ig cell adhesion molecule Basigin controls compartmentalization and vesicle release at Drosophila melanogaster synapses', *The Journal of Cell Biology*, 177: 843-55.
8. Bhattacharya, S., R. Herrera-Molina, V. Sabanov, T. Ahmed, E. Iscru, F. Stober, K. Richter, K. D. Fischer, F. Angenstein, J. Goldschmidt, P. W. Beesley, D. Balschun, K. H. Smalla, E. D. Gundelfinger, and D. Montag. 2017. 'Genetically Induced Retrograde Amnesia of Associative Memories After Neuroplastin Ablation', *Biol Psychiatry*, 81: 124-35.
9. Boczek, T., M. Sobolczyk, J. Mackiewicz, M. Lisek, B. Ferenc, F. Guo, and L. Zylinska. 2021. 'Crosstalk among Calcium ATPases: PMCA, SERCA and SPCA in Mental Diseases', *Int J Mol Sci*, 22: 2785.
10. Bortolozzi, M., and F. Mammano. 2018. 'PMCA2 pump mutations and hereditary deafness', *Neurosci Lett*, 663: 18-24.
11. Brandt, P., R. L. Neve, A. Kammesheidt, R. E. Rhoads, and T. C. Vanaman. 1992. 'Analysis of the tissue-specific distribution of mRNAs encoding the plasma

membrane calcium-pumping ATPases and characterization of an alternately spliced form of PMCA4 at the cDNA and genomic levels', *J Biol Chem*, 267: 4376-85.

12. Carayol, J., R. Sacco, F. Tores, F. Rousseau, P. Lewin, J. Hager, and A. M. Persico. 2011. 'Converging evidence for an association of ATP2B2 allelic variants with autism in male subjects', *Biol Psychiatry*, 70: 880-7.
13. Cardoso, A. R., M. Lopes-Marques, R. M. Silva, C. Serrano, A. Amorim, M. J. Prata, and L. Azevedo. 2019. 'Essential genetic findings in neurodevelopmental disorders', *Hum Genomics*, 13: 31.
14. Carrott, L., M. R. Bowl, C. Aguilar, S. L. Johnson, L. Chessum, M. West, S. Morse, J. Dorning, E. Smart, R. Hardisty-Hughes, G. Ball, A. Parker, A. R. Barnard, R. E. MacLaren, S. Wells, W. Marcotti, and S. D. Brown. 2016. 'Absence of Neuroplastin-65 Affects Synaptogenesis in Mouse Inner Hair Cells and Causes Profound Hearing Loss', *J Neurosci*, 36: 222-34.
15. Desrivieres, S., A. Lourdasamy, C. Tao, R. Toro, T. Jia, E. Loth, L. M. Medina, A. Kepa, A. Fernandes, B. Ruggeri, F. M. Carvalho, G. Cocks, T. Banaschewski, G. J. Barker, A. L. Bokde, C. Buchel, P. J. Conrod, H. Flor, A. Heinz, J. Gallinat, H. Garavan, P. Gowland, R. Bruhl, C. Lawrence, K. Mann, M. L. Martinot, F. Nees, M. Lathrop, J. B. Poline, M. Rietschel, P. Thompson, M. Fauth-Buhler, M. N. Smolka, Z. Pausova, T. Paus, J. Feng, G. Schumann, and Imagen Consortium. 2015. 'Single nucleotide polymorphism in the neuroplastin locus associates with cortical thickness and intellectual ability in adolescents', *Mol Psychiatry*, 20: 263-74.
16. Doganyigit, Z., A. Okan, S. Yilmaz, A. C. Uguz, and E. Akyuz. 2024. 'Gender-related variation expressions of neuroplastin TRAF6, GluA1, GABA(A) receptor, and PMCA in cortex, hippocampus, and brainstem in an experimental epilepsy model', *Synapse*, 78: e22289.
17. Driver, E. C., and M. W. Kelley. 2020. 'Development of the cochlea', *Development (Cambridge, England)*, 147.
18. Elliott, S. J., and C. A. Shera. 2012. 'The cochlea as a smart structure', *Smart Mater Struct*, 21: 64001.
19. Fettiplace, R., and J. H. Nam. 2019. 'Tonotopy in calcium homeostasis and vulnerability of cochlear hair cells', *Hearing Research*, 376: 11-21.
20. Filipek, P. A., J. Juranek, M. Smith, L. Z. Mays, E. R. Ramos, M. Bocian, D. Masser-Frye, T. M. Laulhere, C. Modahl, M. A. Spence, and J. J. Gargus. 2003. 'Mitochondrial dysfunction in autistic patients with 15q inverted duplication', *Ann Neurol*, 53: 801-4.
21. Gong, D., X. Chi, K. Ren, G. Huang, G. Zhou, N. Yan, J. Lei, and Q. Zhou. 2018. 'Structure of the human plasma membrane Ca(2+)-ATPase 1 in complex with its obligatory subunit neuroplastin', *Nat Commun*, 9: 3623.

22. Herrera-Molina, R., K. Mlinac-Jerkovic, K. Ilic, F. Stober, S. K. Vemula, M. Sandoval, N. J. Milosevic, G. Simic, K. H. Smalla, J. Goldschmidt, S. K. Bognar, and D. Montag. 2017. 'Neuroplastin deletion in glutamatergic neurons impairs selective brain functions and calcium regulation: implication for cognitive deterioration', *Scientific reports*, 7: 7273.
23. Herrera-Molina, R., I. Sarto-Jackson, C. Montenegro-Venegas, M. Heine, K. H. Smalla, C. I. Seidenbecher, P. W. Beesley, E. D. Gundelfinger, and D. Montag. 2014. 'Structure of excitatory synapses and GABAA receptor localization at inhibitory synapses are regulated by neuroplastin-65', *J Biol Chem*, 289: 8973-88.
24. Hill, I. E., C. P. Selkirk, R. B. Hawkes, and P. W. Beesley. 1988. 'Characterization of novel glycoprotein components of synaptic membranes and postsynaptic densities, gp65 and gp55, with a monoclonal antibody', *Brain Res*, 461: 27-43.
25. Hill, Irene, Timothy Willmott, Ioulia Skitsa, Christopher Selkirk, Susan Murphy, Philip Gordon-Weeks, and Philip Beesley. 1989. 'Expression of two synapse-enriched glycoproteins, gp65 and gp55, during rat brain development', *Biochemical Society Transactions*, 17: 770-71.
26. Ilic, K., K. Mlinac-Jerkovic, N. Jovanov-Milosevic, G. Simic, N. Habek, N. Bogdanovic, and S. Kalanj-Bognar. 2019. 'Hippocampal expression of cell-adhesion glycoprotein neuroplastin is altered in Alzheimer's disease', *J Cell Mol Med*, 23: 1602-07.
27. Ilic, K., K. Mlinac-Jerkovic, G. Sedmak, I. Rosenzweig, and S. Kalanj-Bognar. 2021. 'Neuroplastin in human cognition: review of literature and future perspectives', *Transl Psychiatry*, 11: 394.
28. Jensen, T. P., A. G. Filoteo, T. Knopfel, and R. M. Empson. 2007. 'Presynaptic plasma membrane Ca²⁺ ATPase isoform 2a regulates excitatory synaptic transmission in rat hippocampal CA3', *J Physiol*, 579: 85-99.
29. Jiang, C. H., M. Wei, C. Zhang, and Y. S. Shi. 2021. 'The amino-terminal domain of GluA1 mediates LTP maintenance via interaction with neuroplastin-65', *Proc Natl Acad Sci U S A*, 118.
30. Klopocki, E., L. M. Graul-Neumann, U. Grieben, H. Tonnies, H. H. Ropers, D. Horn, S. Mundlos, and R. Ullmann. 2008. 'A further case of the recurrent 15q24 microdeletion syndrome, detected by array CGH', *Eur J Pediatr*, 167: 903-8.
31. Kluge, H., and G. E. Kuhne. 1985. 'Preliminary findings on calmodulin-stimulated Ca²⁺-ATPase of erythrocyte ghosts in psychotic patients', *Eur Arch Psychiatry Neurol Sci*, 235: 57-9.
32. Korthals, M., K. Langnaese, K. H. Smalla, T. Kahne, R. Herrera-Molina, J. Handschuh, A. C. Lehmann, D. Mamula, M. Naumann, C. Seidenbecher, W. Zuschratter, K. Tedford, E. D. Gundelfinger, D. Montag, K. D. Fischer, and U. Thomas. 2017. 'A complex of Neuroplastin and Plasma Membrane Ca(2+) ATPase controls T cell activation', *Scientific reports*, 7: 8358.

33. Kozel, Peter J. 1998. 'Balance and Hearing Deficits in Mice with a Null Mutation in the Gene Encoding Plasma Membrane Ca²⁺-ATPase Isoform 2*'.
J Biol Chem, 272: 821-7.
34. Kreutz, M. R., K. Langnaese, D. C. Dieterich, C. I. Seidenbecher, W. Zuschratter, P. W. Beesley, and E. D. Gundelfinger. 2001. 'Distribution of transcript and protein isoforms of the synaptic glycoprotein neuroplastin in rat retina', *Invest Ophthalmol Vis Sci*, 42: 1907-14.
35. Langnaese, K., P. W. Beesley, and E. D. Gundelfinger. 1997. 'Synaptic membrane glycoproteins gp65 and gp55 are new members of the immunoglobulin superfamily', *J Biol Chem*, 272: 821-7.
36. Langnaese, K., R. Mummery, E. D. Gundelfinger, and P. W. Beesley. 1998. 'Immunoglobulin superfamily members gp65 and gp55: tissue distribution of glycoforms', *FEBS Lett*, 429: 284-8.
37. Li, H., Y. Liu, X. Gao, L. Liu, S. Amuti, D. Wu, F. Jiang, L. Huang, G. Wang, J. Zeng, B. Ma, and Q. Yuan. 2019. 'Neuroplastin 65 modulates anxiety- and depression-like behavior likely through adult hippocampal neurogenesis and central 5-HT activity', *FEBS J*, 286: 3401-15.
38. Li, S., X. Wei, H. Huang, L. Ye, M. Ma, L. Sun, Y. Lu, and Y. Wu. 2023. 'Neuroplastin exerts antiepileptic effects through binding to the alpha1 subunit of GABA type A receptors to inhibit the internalization of the receptors', *J Transl Med*, 21: 707.
39. Lin, X., M. G. K. Brunk, P. Yuanxiang, A. W. Curran, E. Zhang, F. Stober, J. Goldschmidt, E. D. Gundelfinger, M. Vollmer, M. F. K. Happel, R. Herrera-Molina, and D. Montag. 2021a. 'Neuroplastin expression is essential for hearing and hair cell PMCA expression', *Brain Struct Funct*, 226: 1533-51.
40. Lin, X., Y. Liang, R. Herrera-Molina, and D. Montag. 2021b. 'Neuroplastin in Neuropsychiatric Diseases', *Genes (Basel)*, 12.
41. Malci, A., X. Lin, R. Sandoval, E. D. Gundelfinger, M. Naumann, C. I. Seidenbecher, and R. Herrera-Molina. 2022. 'Ca(2+) signaling in postsynaptic neurons: Neuroplastin-65 regulates the interplay between plasma membrane Ca(2+) ATPases and ionotropic glutamate receptors', *Cell Calcium*, 106: 102623.
42. Marter, K., O. Kobler, I. Erdmann, E. Soleimanpour, P. Landgraf, A. Muller, J. Abele, U. Thomas, and D. C. Dieterich. 2019. 'Click Chemistry (CuAAC) and Detection of Tagged de novo Synthesized Proteins in Drosophila', *Bio Protoc*, 9: e3142.
43. Martins-de-Souza, D., W. F. Gattaz, A. Schmitt, C. Rewerts, S. Marangoni, J. C. Novello, G. Maccarrone, C. W. Turck, and E. Dias-Neto. 2009. 'Alterations in oligodendrocyte proteins, calcium homeostasis and new potential markers in schizophrenia anterior temporal lobe are revealed by shotgun proteome analysis', *J Neural Transm (Vienna)*, 116: 275-89.

44. Mata, A. M., M. Berrocal, and M. R. Sepulveda. 2011. 'Impairment of the activity of the plasma membrane Ca²⁺(+)-ATPase in Alzheimer's disease', *Biochem Soc Trans*, 39: 819-22.
45. Michaelis, M. L. 1989. 'Ca²⁺ handling systems and neuronal aging', *Ann N Y Acad Sci*, 568: 89-94.
46. Michaelis, M. L., D. J. Bigelow, C. Schoneich, T. D. Williams, L. Ramonda, D. Yin, A. F. Huhmer, Y. Yao, J. Gao, and T. C. Squier. 1996. 'Decreased plasma membrane calcium transport activity in aging brain', *Life Sciences*, 59: 405-12.
47. Michaelis, M. L., K. Johe, and T. E. Kitos. 1984. 'Age-dependent alterations in synaptic membrane systems for Ca²⁺ regulation', *Mechanisms of Ageing and Development*, 25: 215-25.
48. Moreno-De-Luca, A., S. M. Myers, T. D. Challman, D. Moreno-De-Luca, D. W. Evans, and D. H. Ledbetter. 2013. 'Developmental brain dysfunction: revival and expansion of old concepts based on new genetic evidence', *Lancet Neurol*, 12: 406-14.
49. Morris-Rosendahl, D. J., and M. A. Crocq. 2020. 'Neurodevelopmental disorders-the history and future of a diagnostic concept ', *Dialogues Clin Neurosci*, 22: 65-72.
50. Munro, M., Y. Akkam, and K. D. Curtin. 2010. 'Mutational analysis of Drosophila basigin function in the visual system', *Gene*, 449: 50-8.
51. Newton, S., F. Kong, A. J. Carlton, C. Aguilar, A. Parker, G. F. Codner, L. Teboul, S. Wells, S. D. M. Brown, W. Marcotti, and M. R. Bowl. 2022. 'Neuroplastin genetically interacts with Cadherin 23 and the encoded isoform Np55 is sufficient for cochlear hair cell function and hearing', *PLoS Genet*, 18: e1009937.
52. Owczarek, S., D. Kiryushko, M. H. Larsen, J. S. Kastrup, M. Gajhede, C. Sandi, V. Berezin, E. Bock, and V. Soroka. 2010. 'Neuroplastin-55 binds to and signals through the fibroblast growth factor receptor', *FASEB J*, 24: 1139-50.
53. Poggio, E., L. Barazzuol, A. Salmaso, C. Milani, A. Deligiannopoulou, A. G. Cazorla, S. S. Jang, N. Julia-Palacios, B. Keren, R. Kopajtich, S. A. Lynch, C. Mignot, C. Moorwood, C. Neuhofer, V. Nigro, A. Oostra, H. Prokisch, V. Saillour, N. Schuermans, A. Torella, P. Verloo, E. Yazbeck, M. Zollino, R. Jech, J. Winkelmann, J. Necpal, T. Cali, M. Brini, and M. Zech. 2023. 'ATP2B2 de novo variants as a cause of variable neurodevelopmental disorders that feature dystonia, ataxia, intellectual disability, behavioral symptoms, and seizures', *Genet Med*, 25: 100971.
54. Rahimi, M. J., N. Urban, M. Wegler, H. Sticht, M. Schaefer, B. Popp, F. Gaunitz, M. Morleo, V. Nigro, S. Maitz, G. M. S. Mancini, C. Ruivenkamp, E. K. Suk, T. Bartolomeus, A. Merckenschlager, D. Koboldt, D. Bartholomew, A. P. A. Stegmann, M. Sinnema, I. Duynisveld, R. Salvarinova, S. Race, B. B. A. de Vries, A. Trimouille, S. Naudion, D. Marom, U. Hamiel, N. Henig, F. Demurger, N. Rahner, E. Bartels, J. A. Hamm, A. M. Putnam, R. Person, R. Abou Jamra, and H. Oppermann. 2022. 'De

- novo variants in ATP2B1 lead to neurodevelopmental delay', *Am J Hum Genet*, 109: 944-52.
55. Raphael, Y., and R. A. Altschuler. 2003. 'Structure and innervation of the cochlea', *Brain Res Bull*, 60: 397-422.
56. Reiss, A. L. 2009. 'Childhood developmental disorders: an academic and clinical convergence point for psychiatry, neurology, psychology and pediatrics', *J Child Psychol Psychiatry*, 50: 87-98.
57. Rodriguez-Pinto, D., J. Sparkowski, M. P. Keough, K. N. Phoenix, F. Vumbaca, D. K. Han, E. D. Gundelfinger, P. Beesley, and K. P. Claffey. 2009. 'Identification of novel tumor antigens with patient-derived immune-selected antibodies', *Cancer Immunol Immunother*, 58: 221-34.
58. Saito, A., Y. Fujikura-Ouchi, A. Kuramasu, K. Shimoda, K. Akiyama, H. Matsuoka, and C. Ito. 2007. 'Association study of putative promoter polymorphisms in the neuroplastin gene and schizophrenia', *Neurosci Lett*, 411: 168-73.
59. Sakaguchi, M., M. Yamamoto, M. Miyai, T. Maeda, J. Hiruma, H. Murata, R. Kinoshita, I. M. Winarsa Ruma, E. W. Putranto, Y. Inoue, S. Morizane, N. H. Huh, R. Tsuboi, and T. Hibino. 2016. 'Identification of an S100A8 Receptor Neuroplastin-beta and its Heterodimer Formation with EMMPRIN', *J Invest Dermatol*, 136: 2240-50.
60. Sarto-Jackson, I., I. Milenkovic, K. H. Smalla, E. D. Gundelfinger, T. Kaehne, R. Herrera-Molina, S. Thomas, M. A. Kiebler, and W. Sieghart. 2012. 'The cell adhesion molecule neuroplastin-65 is a novel interaction partner of gamma-aminobutyric acid type A receptors', *J Biol Chem*, 287: 14201-14.
61. Schmidt, N., A. Kollwe, C. E. Constantin, S. Henrich, A. Ritzau-Jost, W. Bildl, A. Saalbach, S. Hallermann, A. Kulik, B. Fakler, and U. Schulte. 2017. 'Neuroplastin and Basigin Are Essential Auxiliary Subunits of Plasma Membrane Ca(2+)-ATPases and Key Regulators of Ca(2+) Clearance', *Neuron*, 96: 827-38 e9.
62. Schnorrer, F., C. Schonbauer, C. C. Langer, G. Dietzl, M. Novatchkova, K. Schernhuber, M. Fellner, A. Azaryan, M. Radolf, A. Stark, K. Keleman, and B. J. Dickson. 2010. 'Systematic genetic analysis of muscle morphogenesis and function in *Drosophila*', *Nature*, 464: 287-91.
63. Schultz, J. M., Y. Yang, A. J. Caride, A. G. Filoteo, A. R. Penheiter, A. Lagziel, R. J. Morell, S. A. Mohiddin, L. Fananapazir, A. C. Madeo, J. T. Penniston, and A. J. Griffith. 2005. 'Modification of human hearing loss by plasma-membrane calcium pump PMCA2', *The New England Journal of Medicine*, 352: 1557-64.
64. Sharp, A. J., R. R. Selzer, J. A. Veltman, S. Gimelli, G. Gimelli, P. Striano, A. Coppola, R. Regan, S. M. Price, N. V. Knoers, P. S. Eis, H. G. Brunner, R. C. Hennekam, S. J. Knight, B. B. de Vries, O. Zuffardi, and E. E. Eichler. 2007. 'Characterization of a recurrent 15q24 microdeletion syndrome', *Human Molecular Genetics*, 16: 567-72.

65. Smith, M., M. A. Spence, and P. Flodman. 2009. 'Nuclear and mitochondrial genome defects in autisms', *Ann N Y Acad Sci*, 1151: 102-32.
66. Smits, J. J., J. Oostrik, A. J. Beynon, S. G. Kant, P. A. M. de Koning Gans, L. J. C. Rotteveel, J. S. Klein Wassink-Ruiter, R. H. Free, S. M. Maas, J. van de Kamp, P. Merkus, Doofnl Consortium, W. Koole, I. Feenstra, R. J. C. Admiraal, C. P. Lanting, M. Schraders, H. G. Yntema, R. J. E. Pennings, and H. Kremer. 2019. 'De novo and inherited loss-of-function variants of ATP2B2 are associated with rapidly progressive hearing impairment', *Hum Genet*, 138: 61-72.
67. Sumardika, I. W., Y. Chen, N. Tomonobu, R. Kinoshita, I. M. W. Ruma, H. Sato, E. Kondo, Y. Inoue, A. Yamauchi, H. Murata, K. I. Yamamoto, S. Tomida, K. Shien, H. Yamamoto, J. Soh, J. Futami, E. W. Putranto, T. Hibino, M. Nishibori, S. Toyooka, and M. Sakaguchi. 2019. 'Neuroplastin-beta mediates S100A8/A9-induced lung cancer disseminative progression', *Mol Carcinog*, 58: 980-95.
68. Vemula, S. K., A. Malci, L. Junge, A. C. Lehmann, R. Rama, J. Hradsky, R. A. Matute, A. Weber, M. Prigge, M. Naumann, M. R. Kreutz, C. I. Seidenbecher, E. D. Gundelfinger, and R. Herrera-Molina. 2020. 'The Interaction of TRAF6 With Neuroplastin Promotes Spinogenesis During Early Neuronal Development', *Front Cell Dev Biol*, 8: 579513.
69. Wilson, M. C., M. Kraus, H. Marzban, J. R. Sarna, Y. Wang, R. Hawkes, A. P. Halestrap, and P. W. Beesley. 2013. 'The neuroplastin adhesion molecules are accessory proteins that chaperone the monocarboxylate transporter MCT2 to the neuronal cell surface', *PloS one*, 8: e78654.
70. Zacharias, D. A., and C. Kappen. 1999. 'Developmental expression of the four plasma membrane calcium ATPase (Pmca) genes in the mouse', *Biochimica Et Biophysica Acta*, 1428: 397-405.
71. Zeng, W. Z., N. Grillet, J. B. Dewey, A. Trouillet, J. F. Krey, P. G. Barr-Gillespie, J. S. Oghalai, and U. Muller. 2016. 'Neuroplastin Isoform Np55 Is Expressed in the Stereocilia of Outer Hair Cells and Required for Normal Outer Hair Cell Function', *J Neurosci*, 36: 9201-16.

8. Acknowledgements

Die Danksagung ist in der Version aus Datenschutzgründen nicht enthalten.

Die Danksagung ist in der Version aus Datenschutzgründen nicht enthalten.

9. Ehrenerklärung

Ich erkläre, dass ich die der Medizinischen Fakultät der Otto-von-Guericke-Universität zur Promotion eingereichte Dissertation mit dem Titel

Mutations in *NPTN* could hinder neurodevelopment by impairing the regulation of plasma membrane Ca^{2+} -ATPase (PMCA) levels and Ca^{2+} transients in brain neurons

im Leibniz-Institut für Neurobiologie, Magdeburg

ohne sonstige Hilfe durchgeführt und bei der Abfassung der Dissertation keine anderen als die dort aufgeführten Hilfsmittel benutzt habe.

Bei der Abfassung der Dissertation sind Rechte Dritter nicht verletzt worden.

Ich habe diese Dissertation bisher an keiner in- oder ausländischen Hochschule zur Promotion eingereicht. Ich übertrage der Medizinischen Fakultät das Recht, weitere Kopien meiner Dissertation herzustellen und zu vertreiben.

Magdeburg, den

Unterschrift

Ich erkläre hiermit, nicht wegen einer Straftat verurteilt worden zu sein, die
Wissenschaftsbezug hat.

Magdeburg, den

Unterschrift

10. Curriculum Vitae

Der Lebenslauf ist in der Version aus Datenschutzgründen nicht enthalten.

Der Lebenslauf ist in der Version aus Datenschutzgründen nicht enthalten.

11. Appendix

List of Figures

Figure 1:

Overview of the variant susceptibility landscape for *NPTN* along with the distribution of variants observed in individuals

Figure 2:

Schematic diagram of Np structure

Figure 3:

Schematic diagram of Np binding to different partner molecules

Figure 4:

Schematic illustration of the structure of the inner ear and Ca^{2+} homeostasis in hair cells

Figure 5:

Sequence alignment of Np in human and Bsg in *Drosophila*

Figure 6:

Generation of recombined *Drosophila* lines for Gal4-induced co-expression of bsg-RNAi and hNp55

Figure 7:

Reported mutations from database and alignment of Np sequences across different species

Figure 8:

Schematic illustration of the variant's sites in two hNp isoforms

Figure 9:

Western blot analysis of Np and PMCA in HEK293T cells transfected with PMCA2-GFP or co-transfected with PMCA2-GFP and hNp variants from hNp55/65^{pitch} and hNp55/65^{audio-1}

Figure 10:

Western blot analysis of Np and PMCA in HEK293T cells transfected with PMCA2-GFP or co-transfected with PMCA2-GFP and hNp variants from human patients

Figure 11:

Western blot of PNGaseF treatment from HEK293T cells

Figure 12:

RT-PCR analysis of hNp55/65^{WT}, hNp55/65^{pitch}, hNp55/65^{audio-1}

Figure 13:

Western blot of Proteasomal (MG132) or lysosomal (NH₄Cl) inhibitor treatment from HEK293T cells

Figure 14:

An example of calcium imaging of a hippocampal neuron and schematic diagram of calcium kinetic analysis

Figure 15:

LFS condition calcium imaging analysis in hNp65^{pitch} and hNp65^{audio-1} transfected hippocampal neurons

Figure 16:

HFS condition calcium imaging analysis in variant hNp65^{audio-1} transfected hippocampal neurons

Figure 17:

Immunohistochemical staining and quantification of Np and PMCA intensity in hippocampal neurons

Figure 18:

HFS condition calcium imaging analysis in variants hNp65^{p.W135R}, hNp65^{p.P342L} and hNp65^{p.T194P} transfected hippocampal neurons

Figure 19:

100Hz HFS condition calcium imaging analysis in Np-siRNA and variants hNp65^{p.P342L} or hNp65^{p.T194P} transfected hippocampal neurons

Figure 20:

Immunohistochemical staining examples and quantification of PMCA intensity in *Drosophila* NMJs

Figure 21:

Schematic illustration of interactions between the transmembrane area of hPMCA1 and NPTN

List of Tables

Table 1:

Primer list for all constructs

Table 2:

Reagents and volumes for PCR

Table 3:

PCR amplification program

Table 4:

Reagents for agarose gel electrophoresis

Table 5:

Reagents for Cold fusion cloning procedure

Table 6:

Reagents for Restriction Digestion

Table 7:

Medium list in HEK293T cell culture

Table 8:

Wash solution and Amido Black solution recipe

Table 9:

Western Blot buffer list

Table 10:

Immunocytochemistry buffer list

Table 11:

Calcium imaging buffer list

List of Antibodies

Antibodies	Species	Concentration	Company,Catalogue number
Primary antibodies			
Anti-Neuroplastin	Sheep	IHC: 1:300/500 WB: 1:5,000	RD systems (AF5174)
Anti-β-Actin	Mouse	WB: 1:10,000	Thermo Fisher (A5441)
Anti-GFP	Mouse	WB: 1:10,000	Sigma (11814460001)
Anti-PMCA	Mouse	IHC: 1:500	Invitrogen (MA3-914)
Anti-PMCA	Rabbit	IHC: 1:300	from Dr.U.Thomas
Secondary antibodies			
Anti-sheep cy3	Donkey	IHC: 1:300/1000	Jackson ImmunoResearch Laboratories (713-165-147)
Anti-mouse cy5	Donkey	IHC: 1:300/1000	Jackson ImmunoResearch Laboratories (711-175-151)
Anti-rabbit 488	Donkey	IHC: 1:300	Jackson ImmunoResearch Laboratories (715-175-152)
Anti-Hrp 647	Goat	IHC: 1:300	Jackson ImmunoResearch Laboratories 123-605-021
Anti-rabbit Alexa488	Donkey	IHC: 1:300	from Dr.U.Thomas

List of used Kits

Kits	Company,Catalogue number
NucleoSpin Gel and PCR clean-up Kit	Macherry-Nagel (740611.10)
Cold Fusion™ Cloning Kit	System Biosciences (MC100B-1)
QIAprep Spin Miniprep Kit	Qiagen (27104)
NucleoBond® Xtra Midi EF Kit	Macherry-Nagel (740422.50)
RNeasy Plus Mini Kit	Qiagen (74134)
Chemiluminescent HRP Substrate	Millipore (#WBKLS0500)
